Dear Professor Kienast, dear referee 3,

we have now moved Fig. S2 as new Fig. 5 into the main manuscript and changed the text accordingly (the problem of the citation of Krossa et al. 2017 in wrong context was removed thereby), and we have included a brief discussion. We have also included the TEX86-related formulas in the main text.

Thank you very much for editing/reviewing our manuscript.

Kind regards

Ulrich Kotthoff

Reconstructing Holocene temperature and salinity variations in the western Baltic Sea region: A multi-proxy comparison from the Little Belt (IODP Expedition 347, Site M0059)

Ulrich Kotthoff[1,2], Jeroen Groeneveld[3], Jeanine L. Ash[4], Anne-Sophie Fanget[5,6], Nadine Quintana Krupinski[7], Odile Peyron[8], Anna Stepanova[9], Jonathan Warnock[10], Niels A. G. M. Van Helmond[11], Benjamin H. Passey[12], Ole Rønø Clausen[5], Ole Bennike[13], Elinor Andrén[14], Wojciech Granoszewski[15], Thomas Andrén[14], Helena L. Filipsson[7], Marit-Solveig Seidenkrantz[5], Caroline P. Slomp[11], Thorsten Bauersachs[16]

[1]Institute for Geology, University of Hamburg, D-20146, Hamburg, Germany

[2]Center of Natural History, University of Hamburg, D-20146, Hamburg, D-20146, Germany

[3]MARUM, Center for Marine Environmental Sciences, University of Bremen, D-28359, Bremen, Germany

[4]Department of Earth, Planetary, and Space Sciences, UCLA, US-90024, USA

[5]Centre for Past Climate Studies, Department of Geoscience, Aarhus University, DK-8000 Aarhus C, Denmark

[6]Centre de formation et de recherche sur les environnements méditerranées, Université de Perpignan, FR-66860, Perpignan cedex, France

[7]Department of Geology, Lund University, SE-22362 Lund, Sweden

[8]Institute of Evolutionary Sciences, UMR 5554, University of Montpellier, FR-34095 Montpellier cedex 05, France

[9]Department of Computer Science and Engineering, Texas A&M University, US-77843, USA

[10]Department of Geoscience, Indiana University of Pennsylvania, US-15705, USA

[11]Department of Earth Sciences - Geochemistry, Faculty of Geosciences, Utrecht University. PO Box 80021, NL-3508 TA Utrecht, Netherlands

[12]Department of Earth and Environmental Sciences, University of Michigan, US-48109, USA

[13]Geological Survey of Denmark and Greenland, DK-1350 Copenhagen, Denmark

[14]School of Natural Sciences, Technology and Environmental Studies, Södertörn University, SE-14189 Huddinge, Sweden

[15]Polish Geological Institute-National Research Institute Krakow, PL-31-560 Krakow, Poland

[16]Christian-Albrechts-University, Institute of Geosciences, Department of Organic Geochemistry, D-24118 Kiel, Germany

Correspondence to: Ulrich Kotthoff (ulrich.kotthoff@uni-hamburg.de)

Abstract

Sediment records recovered from the Baltic Sea during Integrated Ocean Drilling Program Expedition 347 provide a unique opportunity to study paleoenvironmental and -climate change in central/northern Europe. Such studies contribute to a better understanding of how environmental parameters change in continental shelf seas and enclosed basins. ~~We~~Here we present a multi-proxy-based reconstruction of paleotemperature (both marine and terrestrial), -salinity, and -ecosystem changes from the Little Belt (Site M0059) over the past ~8,000 years, and evaluate the applicability of inorganic- and organic-based proxies in this particular setting.

All salinity proxies (diatoms, aquatic palynomorphs, ostracods, diol index) show that lacustrine conditions occurred in the Little Belt until ~7,400 cal. yr BP. A connection to the Kattegat at this time can thus be excluded, but a direct connection to the Baltic Proper may have existed. The transition to the brackish-marine conditions of the Littorina Sea stage (more saline and warmer) occurred within ~200 yr when the connection to the Kattegat became established (~~,~~ after ~7,400 cal. yr BP~~),~~. The different salinity proxies used here generally show similar trends in relative changes in salinity, but often do not allow quantitative estimates of salinity.

The reconstruction of water temperatures is associated with particular large uncertainties and variations in absolute values by up to 8 °C for bottom waters and up to 16 °C for surface waters. Concerning the reconstruction of temperature using foraminiferal Mg/Ca-ratios, contamination by authigenic coatings in the deeper intervals may have led to an over-estimation of temperatures. Differences in results based on the lipid paleothermometers (long chain diol index and TEX^L_{86}) can partly be explained by the application of modern-day proxy calibrations to intervals which experienced significant changes in depositional settings, in case of our study e.g. change from freshwater to marine conditions. Our study shows that particular caution has to be taken when applying and interpreting proxies in coastal environments and marginal seas, where water mass conditions can experience more rapid and larger changes than in open-ocean settings. Approaches using a multitude of independent proxies may thus allow a more robust paleoenvironmental assessment.

1 Introduction

Recent climate change is showing a persistent trend to a more positive state of the North Atlantic Oscillation resulting in wetter conditions especially over northern Europe (Hurrell, 1995; Visbeck et al., 2001). Further increased westerly winds together with a changed barotrophic pressure gradient may result in increased inflows of open-marine waters and therewith more saline deep waters in the Baltic Sea in the future (cf. Meier et al., 2006; Meier, 2015). Concomitantly, the increase in continental runoff due to increased precipitation may result in a freshening of the surface waters in the Baltic Sea (Matthäus and Schinke, 1999; Gustafsson and Westman, 2002).

Both temperature and salinity changes will thus have important consequences for the Baltic Sea environment (e.g. Meier et al., 2012). To improve our understanding of the impact and magnitude of future environmental changes in the Baltic Sea

65 region, it is essential to generate high-resolution paleo-reconstructions in order to investigate how salinity and temperature varied in the past (e.g. Zillén et al., 2008; Andrén et al., 2015a; Ning et al., 2017). A multi-proxy approach, comprising proxies representative for bottom water, surface water and air (terrestrial) conditions, is used here to reconstruct a wide array of environmental change (in particular temperature and salinity) from the same or closely neighbouring samples, and thus, how conditions simultaneously changed within the same age constraints.

70 The occurrence of specific species of ostracods and foraminifera are important indicators of bottom water parameters, in case of the Baltic Sea primarily salinity (Lutze, 1965; 1974; Murray, 2006; Frenzel and Boomer., 2005; 2010; Viehberg et al., 2008). Additionally, stable oxygen and possibly carbon isotopes in foraminifera are commonly related to changes in salinity, though stable oxygen isotopes are also influenced by temperature and global ice volume, while productivity is another control factor for carbon isotopes (Kristensen and Knudsen, 2006; Filipsson et al., 2016). Bottom water temperatures can be

75 reconstructed using Mg/Ca in benthic foraminifera (Raitzsch et al., 2008), but large gradients in salinity (and low absolute salinity) as well as parameters related to the carbonate system (e.g. alkalinity and carbonate saturation state) in the Baltic Sea may significantly influence the application of Mg/Ca ratios (Groeneveld and Filipsson, 2013).

Due to the low salinity and overall shallowness of the Baltic Sea, planktonic foraminifera are absent from the Baltic Sea region (Seidenkrantz, 1993; Andrén et al., 2015a). Diatoms and marine palynomorphs like dinoflagellates, however, are common and

80 often very good indicators of changes in salinity (Andrén et al., 2000; Snoeijs and Weckström, 2010; Ning et al., 2015).

A proxy which appears to be only dependent on temperature and may therefore be ideal for the Baltic Sea are clumped isotopes on molluscs (Henkes et al., 2013; Wacker et al., 2014). This proxy has not yet been applied to samples from the Baltic Sea. 'Clumped isotopes' (or, more correctly, 'clumped isotopologues') are isotopic molecules that contain more than one rare isotope (e.g. the carbonate isotopologue $Ca^{13}C^{18}O^{16}O_2$). The abundance of these molecules in carbonate is determined by the formation

85 temperature of the mineral.

The lipid paleothermometer TEX_{86} (TetraEther index of tetraethers consisting of 86 carbon atoms), based on the sedimentary distribution of isoprenoid glycerol dialkyl glycerol tetraethers (GDGTs) produced by pelagic Thaumarchaeota, has been successfully used in the reconstruction of sea water temperatures in numerous paleoceanographic settings (Schouten et al., 2002; 2013). A derivative of this proxy is the TEX^L_{86}, which in low temperature environments (generally below 15 °C) shows

90 a high correlation with sea surface temperature (SST; Kim et al., 2010). In the Baltic Sea, the TEX^L_{86} has been shown to be best correlated with late summer SSTs and used to investigate climate-induced variations in water temperature over the past ~1,000 yr (Kabel et al., 2012), while complete TEX^L_{86} records of Holocene climate change are yet missing. A more recently introduced proxy that shows promise in paleoenvironmental studies is the long chain diol index (Rampen et al., 2012). This proxy makes use of the sedimentary distribution of long chain diols synthesized by eustigmatophytes and has been suggested

95 to either reflect an annual (Rampen et al., 2012; de Bar et al., 2016) or a summer SST signal (Lopes dos Santos et al., 2013) in marine settings. In addition to SST, however, salinity has been observed to also affect the distribution of long chain diols in aquatic environments and consequently the diol index has been proposed as a tool to qualitatively assess relative changes in freshwater input to marine environments (Versteegh et al., 1997). An alternative mean to investigate past climate dynamics is

provided by terrestrial palynomorphs such as pollen grains. The modern analogues technique (MAT) and similar approaches

100   furthermore allow calculating quantitative climate data (e.g. temperature, precipitation, seasonality) from pollen assemblages (e.g. Guiot, 1990; Kotthoff et al., 2008; 2011).

Despite a large amount of proxy-based research performed in the Baltic Proper (e.g. Zillén et al., 2008; and references therein; Kotilainen et al., 2014), there are no continuous records from the Baltic Sea and its connections to the Kattegat (Little Belt, Great Belt, and Öresund) enabling multi-proxy studies in high temporal resolution for the entire Holocene (Andrén et al.,

105   2015a), and particularly the Holocene history of the Little Belt has not been in the focus of research (Bennike and Jensen, 2011). Continuous high-resolution records would not only allow correlation between the different basins in the Baltic Sea region but also provide a connection to terrestrial archives.

In the framework of International Ocean Drilling Program (IODP) Expedition 347, a series of long, continuous sediment records in the Baltic Sea region was recovered that allows reconstructing environmental change in central/northern Europe in

110   an unprecedented manner (Andrén et al., 2015a, b). Here we present a centennial-resolution multi-proxy study of IODP Expedition 347 Site M0059 from the Little Belt, one of the connections between the Baltic Sea and the North Sea, using a variety of different proxies which are commonly used in paleoceanography to reconstruct past sea water temperature and salinity. We investigate how these proxies perform in a proximal setting like the Little Belt and how they link to seasonality. We selected the last ~8,000 yr at Site M0059 (top ~53 m of sediment) which include the transition from freshwater to

115   brackish/marine conditions. We show that a multi-proxy approach allows unravelling the different factors which have influenced past conditions in the Little Belt, suggesting that its history may have been partly different from that of the Baltic Proper.

2 Regional setting and methods

2.1 Regional setting

120   The Baltic Sea is connected to the North Sea by the Belt Seas, including the Öresund, the Great Belt, and the Little Belt through the Kattegat and Skagerrak. It is one of the world's largest brackish water bodies, with a surface water salinity ranging from close to zero in the innermost parts of the Gulf of Finland, seven in the Baltic Proper and between 8 and 24 in the Belt Sea. A halocline, varying between 20 and 80 m water depth in the different subbasins, separates the upper water masses from more saline bottom waters. The mean water depth is 54 m, varying between 25 and 200 m with the deepest basin, the Landsort Deep

125   (central Baltic Sea) having a maximum depth of 459 m (e.g. Leppäranta and Myrberg, 2009). The Baltic Sea basin is surrounded by two biomes, from temperate forest with mixed coniferous and broad-leaved trees in the south to boreal forest with taiga-like conditions in the north.

Currents in the Little Belt consist of either relatively low salinity (14-17) surface water flowing out of the Baltic Sea into the Kattegat or higher salinity (>24) currents flowing into the Baltic Sea. Depending on the volume and mixing rate the denser,

130 inflowing water sinks after passing the main sills and can therefore be encountered at different water depths in the Baltic Proper. Because the Baltic Sea has a surplus of freshwater input, i.e. the input of water by precipitation and rivers exceeds evaporation, a positive barotropic pressure gradient exists between the Baltic Proper and the Kattegat, so that under 'normal' conditions surface waters flow from the Baltic Proper into the Kattegat (HELCOM, 1986; Jakobsen and Ottavi, 1997). The contribution of water mass transport through the Little Belt is minor (<10%) in comparison to the Great Belt and the Öresund

135 (HELCOM, 1986). Occasionally the surface flow reverses and more saline water enters over the sills into the straits (Matthäus and Schinke, 1999; Mohrholz et al., 2015). The higher salinity causes the inflowing water to sink and continue as subsurface water into the Baltic Proper. Because the Little Belt is very narrow, with high current velocity and turbulence, a major marine inflow from the Kattegat can lead to mixing of the water column (Jakobsen and Ottavi, 1997).

Mean surface water salinity in the Little Belt was 15.9±0.4 for a 10-yr period (2004-2014), varying between 14.2±0.9 in spring

140 and 17.6±1.5 in autumn, while mean bottom water salinity was 23.6±1.0 varying between 21.5±0.9 in winter and 25.2±1.1 in summer (ICES, 2017). During the same time period, the mean annual SST was 10.6±0.6 °C (ICES, 2017). The mean winter SST was 2.5±1.5 °C, while the mean summer SST was 17.6±0.7 °C with maximum water temperatures of 21-22 °C observed from late July to mid-August (ICES, 2017). Bottom water temperatures averaged 7.6±0.6 °C and varied between 4.3±0.7 °C in winter and 9.3±1.3 °C in summer (ICES, 2017).

145 The Baltic Sea region has experienced several climate-driven hydrological changes during the Holocene. Its history is highly dynamic and governed by the regional isostatic rebound and global sea level changes resulting in alternating freshwater and brackish phases and complex shoreline development (e.g. Björck, 2008; Knudsen et al., 2011; Andrén et al., 2011). The time interval investigated in this study comprises the transition from freshwater to the brackish-marine conditions of the Littorina Sea stage to the present brackish Baltic Sea. In the Baltic Proper, the Baltic Ice Lake (~16,000 to ~11,700 cal. yr BP) was

150 followed by the partly brackish Yoldia Sea stage (~11,700 to ~10,700 cal. yr BP), the lacustrine Ancylus Lake stage (~10,700 to 10,200 cal. yr BP), a transitional low salinity phase (~10,200 to ~7,400 cal. yr BP), and by the Littorina stage (~7,400 cal. yr BP; e.g. Sohlenius et al., 1996; Andrén et al., 2000; Björck, 2008; Andrén et al., 2011).

2.2 Material and methods

155 During IODP Expedition 347, cores were recovered from five holes (A to E) at Site M0059 (Little Belt; Fig. 1), at ~37 m water depth (55°0.29′N, 10°6.49′E). The results of our multi-proxy analyses are based on sediments from Holes A, C, D, and E. For most proxies, ~35 samples have been analysed.

2.2.1 Sedimentology and age model

The sedimentology of Holes M0059A, D, and E was assessed in the framework of the expedition's onshore science party

160 (Andrén et al., 2015a, b). The sedimentary sequence of IODP Site M0059 has been divided into seven lithostratigraphic units

based on visual core descriptions and smear slide analyses (Andrén et al., 2015a), from which subunits Ia and Ib have been investigated in this study. Subunit Ia (0-49.37 meters composite depth – mcd) is composed of mostly homogeneous black to greenish black clay, with some millimetre-scale laminations. It was deposited under brackish-marine conditions, as indicated by diatom assemblages (Andrén et al., 2015a; Fig. 2). Subunit Ib (49.37-53.57 mcd) is a continuation of Subunit Ia. Its base

165 consists of 10-15 cm of black, laminated clays. The remainder of Unit Ib comprises greenish to gray, silty clay, intercalated by centimetre-scale pale green laminae. The presence of freshwater diatoms indicates lacustrine conditions (Andrén et al., 2015a, Fig. 2). Magnetic susceptibility data (supported by natural gamma ray and gamma ray attenuation density data) collected from Holes M0059A-E were used to correlate between each hole and to construct a composite splice section for IODP Site M0059 including a meters composite depth (mcd) scale (Andrén et al., 2015a), which was used in this study.

170 The age model for IODP Site M0059 is based on 16 radiocarbon dates derived from bivalve fragments and intact bivalve specimens (*Abra alba*, *Macoma balthica*; Table 1; supplement Table S3S1). Age-depth modelling was performed with CLAM (version 2.2; Blaauw, 2010) with 2000 iterations using the Marine13 calibration dataset (Reimer et al., 2013) and with a deviation (ΔR) of -90 ± 53 from the Marine13 reservoir age. A detailed description of the age reconstruction is given by Van Helmond et al. (2017). Below 48.64 mcd, the ages have been extrapolated linearly, assuming a constant sedimentation rate,

175 because no material suited for dating purposes was recovered from the deeper sections of the sediment sequence. In order to confirm the precision of the ^{14}C-based age model, we have biostratigraphically compared the marine pollen record from IODP Site M0059 (Fig. 2; see below) with a pollen record from varved sediments in Lake Belau in northern Germany (Fig. 1; Dörfler et al., 2012).

180 Table 1: AMS radiocarbon dates from Expedition 347, Site M0059, for more detailed information compare Table S3S1 (supplement) and van Helmond et al. (2017).

Laboratory ID (LuSNo)	Mean composite depth (m)	Material dated	[14]C Age (yr)	Error (yr)	Calibrated age (yr; median)
11289	2.84	*Abra alba*	700	35	405
11476	4.97	*Abra alba*	1265	35	899
11291	8.79	*Abra alba*	1585	35	1213
11292	14.24	*Macoma balthica*	2740	40	2556
11477	21.14	*Macoma balthica*	3780	35	3829
11295	23.49	*Macoma balthica*	4035	40	4187
11479	26.60	*Macoma balthica*	4395	40	4664
11297	27.03	*Macoma balthica*	4500	40	4785
11480	28.20	*Macoma balthica*	4540	40	4845
11300	29.51	*Macoma balthica*	4780	40	5147
11481	31.80	*Macoma balthica*	4890	40	5313
11482	34.05	*Abra alba*	5155	40	5603

11301	35.39	*Abra alba*	5415	40	5885
11483	38.04	*Abra alba*	5770	40	6289
11303	39.75	*Macoma balthica*	6130	40	6662
11304	48.64	bivalve fragments	6845	45	7437

2.2.2 Geochemistry

In order to measure the total organic carbon (TOC) content, sediment samples from Holes C and E were freeze-dried, powdered
185 and homogenized using an agate mortar and pestle. About 0.3 g of powdered sediment per sample was decalcified using 1M
HCl. Subsequently the samples were washed repeatedly with milliQ water after which they were dried for 72 h at 60 °C.
Finally, the samples were powdered and homogenized again, after which they were measured using a Fisons Instruments NA
1500 NCS analyser at Utrecht University, the Netherlands. Results were normalized to international standards and TOC was
calculated upon correction for weight loss by decalcification. The average analytical uncertainty of 0.07 wt.% was calculated
190 based on duplicate analysis of sediment samples (Van Santvoort et al., 2002).

2.2.3 Palynology and pollen-based quantitative climate reconstructions

For the analysis of terrestrial and marine palynomorph assemblages, 36 samples of ~1 cm thickness were taken from 0 to ~53
mcd. Per sample, 1 to 6 g of sediment was processed using standard palynological techniques (HCl and HF treatment and
195 sieving with 7-µm mesh) for marine sediments (e.g. Kotthoff et al., 2008). *Lycopodium* marker spores were added to the
samples in order to calculate palynomorph concentrations (Stockmarr 1971; Fig. 2, Fig. 3). When possible, >200 terrestrial
palynomorphs (excluding spores and bisaccate pollen grains) were determined and counted per sample under 400 to 1000x
magnification. In addition, organic-walled dinoflagellate cysts (dinocysts; as indicators for marine conditions; e.g. de Vernal
and Marret, 2007) and freshwater algae (as indicators for freshwater influence; e.g. Mudie et al., 2002) were determined and
200 counted when occurring. We did not aim at counting a certain sum of dinocysts per samples, since their absolute amount varied
greatly over the analysed interval. On average, 50 dinocysts were identified per sample. This relatively low value is explained
by the general rarity of dinocysts in some samples and relatively low dinocyst diversity in the Baltic Sea (e.g. Ning et al.,
2016).

Quantitative climate data were calculated from pollen data using the Modern Analogue Technique (MAT; e.g. Guiot, 1990).
205 For this technique numerical methods are used to identify recent analogues for fossil pollen assemblages (e.g. Guiot, 1990;
Kotthoff et al., 2008; 2011). Climate conditions for the best modern analogues are considered to be most similar to the
conditions during which the fossil pollen assemblage was deposited. The MAT reconstructions are based on a database with
>3500 modern pollen spectra from Europe (Bordon et al., 2009) and the Mediterranean area (Dormoy et al., 2009). Here we
used the ten modern assemblages with smallest chord distances for the reconstructions of the climate parameters. Bisaccate

210 pollen was removed from the evaluated samples and the database due to its over-representation in marine pollen records (e.g. Kotthoff et al., 2008).

2.2.4 Diatoms

Sediment samples (n = 36; thickness: 1cm) for diatom analysis were freeze-dried. Subsequently, a known mass of sediment, between 0.03 and 0.07 g dry weight, was subsampled from each sample and treated according to Warnock and Scherer (2015).

215 Briefly, sediments were cleaned with dilute HCl to remove carbonates and 10 % H_2O_2 to remove organic carbon. The resultant sediment slurry was disbursed in a 2 L square cross-section beaker containing distilled water and a small glass table with known area including a coverslip, allowing for ultimate abundance determination. Coverslips were dried and permanently mounted to glass slides with the mounting media Naphrax (refractive index = 1.65).

Each slide was counted to a minimum of 300 vegetative diatom valves. Absolute diatom abundance (ADA) can be calculated

220 by counting the number of fields of view needed to reach 300 diatoms and scaling the number of diatoms counted in that known area relative to the total amount of surface area the sample settled onto and the original dry weight of the sediment sample (Warnock and Scherer, 2015). Diatoms were identified to species level according to Snoeijs et al. (1993-1998), Krammer and Lange-Bertalot (1986-1991), and Patrick and Reimer (1966). The salinity preferences and life forms (benthic or pelagic) of diatoms were classified according to Snoeijs et al. (1993-1998, compare ~~Tab. S5~~Table S2). All slides were analysed

225 using differential interference contrast at 1000x magnification and oil immersion. *Chaetoceros* resting spores (CRS) were counted, but not identified to the species level and were not included in the absolute diatom abundance calculations for this study. Analysis of variance (ANOVA) was used to evaluate the differences between the means of these data, accompanied by a Tukey-Kramer test to evaluate pair-wise relationships (for all statistical tests α = 0.05). Because data derived from sediment cores is inherently chronological the results of pairwise tests are only reported for adjacent environment zones (EZs). All

230 statistical relationships were evaluated using PAST v. 3.10 (Hammer et al., 2001).

2.2.5 Benthic Foraminifera

Thirty-six samples of 2-cm sediment thickness (20 cm^3 sediment) were prepared for foraminiferal analyses and wet-sieved through sieves with 63, 100 and 1000 µm mesh. Each fraction was subsequently dried at 40 °C and weighed. The 100-1000 µm fraction was used for the foraminiferal assemblage analysis. In samples with a high concentration of mineral grains, the

235 100-1000 µm fraction of the samples was subjected to heavy liquid treatment using the heavy liquid tetrachlorethylene (C_2Cl_4) with a specific gravity of 1.6 g/cm^3 to separate foraminiferal tests from mineral grains prior to analysis. The residual fraction after heavy liquid separation was checked for foraminifera; only very few specimens were found and thus only the 100-1000 µm light fraction was used for foraminiferal analyses. To ensure statistical validity of the assemblages, a minimum of 300 individual foraminifera were counted from each sample, when possible. Benthic foraminifera were counted and identified to

species level to characterise the faunal assemblages. The benthic foraminiferal concentrations were calculated as number of specimens/cm^3 sediment.

2.2.6 Ostracods

Ostracods were divided into predominant ecological groups and used their ecological data to reconstruct paleosalinity. A total of 75 samples (each comprising 30 cm^3) were processed for ostracod analysis. Since ostracod material was not abundant enough to produce reliable percentage data, we used the total abundance of ostracods per 30 cm^3. Samples were freeze-dried and washed over a 63-µm sieve and subsequently oven dried in paper filters at 40–50 °C. Ostracods were picked from the entire sample residues and their valves identified and counted.

Two ecological classes of ostracods in relation to salinity were distinguished based on ecological data and distribution of modern taxa in the Baltic Sea and adjacent areas (Frenzel et al., 2010): freshwater and brackish-marine. Among brackish-marine ostracods very shallow and deeper water species were distinguished based on ecological data (Frenzel et al., 2010). Predominance of a very shallow water group implies salinity above 6-10, and an environment such as a lagoon, estuary or very shallow water open sea. The deeper-living ecological group includes species that can be found in the open sea environments at both very shallow and deeper locations with salinity > 7-14.

2.2.7 Stable isotopes in foraminifera

Stable oxygen and carbon isotope (δ^{18}O, δ^{13}C) measurements for 36 samples were performed on 10-20 specimens (100-1000 µm fraction) of *Elphidium selseyense* and *Elphidium incertum*. The analyses were performed on a Finnigan MAT 251 gas isotope ratio mass spectrometer equipped with a Kiel I automated carbonate preparation device at the MARUM, University of Bremen, Germany. The stable isotopic data were calibrated relative to the Vienna Peedee belemnite (VPDB) using the NBS19 standard. The standard deviation of the house standard (Solnhofen limestone) over the measurement period was 0.03 ‰ for δ^{13}C and 0.06 ‰ for δ^{18}O.

2.2.8 Trace metal/calcium in foraminifera

Up to 40 specimens (>150 µm) of *E. selseyense* and 25 specimens of *E. incertum* (>150 µm) were selected for trace metal/calcium analysis. If the number of specimens was not sufficient, both species were combined. Due to poor preservation, not enough specimens were present for the analysis of Mg/Ca ratios in depths <5 and >30 mcd. Trace metal/Ca in foraminifera from the Nordic/Baltic Seas has been shown to be occasionally affected by diagenetic coatings (Groeneveld and Filipsson, 2013; Ezat et al., 2016). Standard cleaning procedures for trace metal/Ca in foraminifera after clay removal either involve only an oxidation step to remove organic matter (Barker et al., 2003) or also include a reduction step before the oxidation (Martin and Lea, 2002) to remove (oxy)hydroxide coatings. Both methods, however, triggered a reaction on samples of Site M0059 which turned the foraminiferal fragments (dark) brownish. This suggests that an additional contaminating phase was present

270 on the foraminiferal tests which was not removed by reduction but does respond to oxidation. A likely source for this are (Fe)-sulfides, which are easily formed in Baltic sediments including the Little Belt and adsorb cations (Raiswell and Canfield, 1998; Hardisty et al., 2016; Van Helmond et al., 2017). Oxidation would then turn the (Fe)-sulfide into an (Fe)-hydroxide, which has a brownish color. To remove this phase from the foraminiferal tests the standard combination of reduction and oxidation was reversed. First, oxidation was performed to form the hydroxide, followed by a reduction step to remove this again. As reducing

275 agent 0.1 M hydroxylamine-hypochloridhydrochlorid buffered in a 1 M Na-acetate solution was used (Shen et al., 2001; Steinke et al., 2010). 250 µl reducing agent was added to the samples; the samples were heated for 30 min. at 70° C, and rinsed three times with Seralpur water. After cleaning, the samples were dissolved and centrifuged for 10 minutes (6000 rpm) to exclude any remaining insoluble particles from the analyses. The samples were diluted with Seralpur water before analysis with Inductively Coupled Plasma-Optical Emission Spectrometry (ICP-OES; Agilent Technologies, 700 Series with

280 autosampler ASX-520 Cetac and micro-nebulizer) at MARUM, University of Bremen, Germany. Instrumental precision was monitored after every five samples by analysis of an in-house standard solution with a Mg/Ca of 2.93 mmol/mol (standard deviation of 0.020 mmol/mol or 0.67 %). A limestone standard (ECRM752-1, reported Mg/Ca of 3.75 mmol/mol) was analysed to allow inter-laboratory comparison (Greaves et al., 2008; Groeneveld and Filipsson, 2013). The long-term average of the ECRM752-1 standard, which is routinely analysed twice after every 50 samples in every session, is 3.78 ±0.073 mmol/mol.

285 Analytical precision for *Elphidium* spp. was 0.08 % for Mg/Ca. Reproducibility using replicates of the same samples but cleaned separately was +/- 0.17 mmol/mol (n = 18). Potential contamination was monitored using Al/Ca (clays), Mn/Ca, and Fe/Ca (both for diagenetic coatings) (see supplement Tab. S3 and Fig. S1 for details).

Mg/Ca values reach numbers which are comparable to modern core top analyses of the same species (Groeneveld and Filipsson, unpublished data). Mg/Ca values before 4,000 cal. yr BP, however, are still relatively high, suggesting that the

290 cleaning did not fully remove the contamination. Although FeS and FeS$_2$ are present in the studied sediments of Site M0059 (Van Helmond et al., 2017), it remains unclear what specific kind of sulfide would have been present on the foraminiferal fragments as Fe/Ca did not vary between the different methods (Fig. S1 in Supplementsupplement). Mean Mn/Ca was much lower for the samples in the oxidation-reduction series (10.09 vs 14.81 mmol/mol; Table S3 in Supplement;and Fig. S1 in Supplementsupplement), but these are still values which are much higher than commonly accepted for uncontaminated

295 foraminiferal calcite (Barker et al., 2003). It is possible that the high Mn/Ca values are truly part of the primary foraminiferal calcite and relate as such to redox conditions in the sediment. Groeneveld and Filipsson (2013) showed Mn/Ca values as high as 10.58 mmol/mol in living specimens of *Globobulimina turgida* from the hypoxic zone in the Gullmar Fjord. For future work it may be required to perform a second reduction step instead of just the one step performed here.

2.2.9 Clumped isotopes in molluscs

300 The analyte for clumped isotope thermometry in the case of carbonate is CO_2 liberated by acid digestion, where Δ_{47} is the measure of the amount of mass-47 isotopologues of CO_2 (primarily $^{13}C^{18}O^{16}O$) relative to that predicted by a random

arrangement of atoms (Dennis et al., 2011; Eiler, 2011). A robust relationship between Δ_{47} and the formation temperature of marine molluscs has been determined (Henkes et al., 2013). We measured the clumped isotope composition of mollusc material from Holes M0059A and D and report Δ_{47} inferred temperatures for eleven samples. Mollusc material was separated from

305 sediment samples (~3 cm thickness) by wet sieving. A cold, ten-minute soak of dilute H_2O_2 was used for samples where organic matter was particularly difficult to remove. All samples were triple-rinsed in distilled water and hand cleansed with brushes under a microscope. After species identification, samples were ground in a mortar and pestle and analysed at Johns Hopkins University (USA) on a Thermo Scientific MAT-253 isotope ratio mass spectrometer coupled to an automated acid digestion and CO_2 purification system as described in Henkes et al. (2013). Samples were analysed (3-7 replicates, as material

310 permitted) alongside carbonate standards of varying composition and CO_2 gases approaching equilibrium at 1000 °C and 30 °C, from January to March 2016 (see supplementary material).. Measurements of the temperature-equilibrated CO_2 gas samples were used to create an absolute reference frame for normalization of Δ_{47} values (Dennis et al., 2011), with the calculations performed using a MATLAB® script that accounts for temporal drift in analytical conditions (Passey et al., 2010). Finally, we used the following empirically determined relationship between mollusc Δ_{47} and temperature (Henkes et al., 2013)

315 to convert our measured Δ_{47} to paleotemperatures: $\Delta_{47} = 0.0327 \times 10^6/T^2 + 0.3286$.

2.2.10 Biomarkers

A total of 40 sediment samples collected from Holes M0059A and D was analysed for their lipid biomarker content. For this, ~1-5 gram of sediment (~0.5 cm thickness) was freeze-dried and extracted using a modified Bligh & Dyer technique (Rütters et al., 2002). An aliquot of each Bligh and& Dyer extract (~5 mg) was separated into an apolar and polar fraction using column

320 chromatography with activated Al_2O_3 as stationary phase and n-hexane:DCM (9:1, v:v) and DCM:MeOH (1:1) as respective eluents. The polar fractions were subsequently dried under a gentle stream of N_2 and separated into two aliquots for analyses of glycerol dialkyl glycerol tetraethers (GDGTs) and long chain diols, respectively.

To analyse the GDGT content, aliquots of the polar fractions were dissolved in n-hexane:2-propanol (99:1; v/v) and passed through a 0.4 μm polytetrafluoroethylene (PTFE) filter. Analysis of GDGTs was performed using an Alliance 2695 (Waters,

325 UK) high performance liquid chromatograph (HPLC) coupled to a ZQ (Micromass, UK) single quadrupole mass spectrometer (MS) as detailed in Zink et al. (2016) following the analytical protocols of Hopmans et al. (2000) and Liu et al. (2012). Isoprenoid and branched GDGTs were detected using single ion recording of their protonated molecules $[M+H]^+$ as outlined in Schouten et al. (2013a). The TEX_{86} and. TEX^L_{86} and TEX^H_{86} were calculated using the equations given by Schouten et al. (2002) and Kim et al. (2010):

330

TEX_{86} = TEX^L_{86} = log([GDGT-2] / ([GDGT-1] + [GDGT-2] + [GDGT-3]))

[1]

$$\text{TEX}^H_{86} = \log(([GDGT\text{-}2] + [GDGT\text{-}3] + [Cren']) / ([GDGT\text{-}1] + [GDGT\text{-}2] + [GDGT\text{-}3] + [Cren']) \quad \text{[1]})) \quad [2]$$

$$\text{TEX}^L_{86} = [GDGT\text{-}2] / ([GDGT\text{-}1] + [GDGT\text{-}2] + [GDGT\text{-}3]) \quad [2]$$

TEX^L_{86} values were transferred to absolute temperatures in the brackish-marine sediments of ~~subunit Ia~~EZ2-4 using the Baltic Sea surface sediment calibration (equation ~~3~~4), which is best correlated with late summer SSTs (Kabel et al., 2012). In addition, SSTs (equation 4) and subsurface water temperatures (equation 5) were calculated using the calibrations of Kim et al (2010) and Kim et al. (2012), respectively. In the freshwater interval of ~~subunit Ib~~EZ1, we used the ~~global~~summer lake surface temperature (SLST) calibration (equation ~~4~~6) of Powers et al. (2010) to convert TEX_{86} values in water temperatures. ~~We specifically apply and discuss the summer lake surface temperature (SLST) calibration here but also provide information on the annual and winter lake surface temperature variation in the supplementary material.~~ ..

$$\text{SST} = 34.\underline{}\sim\!\!030 * \text{TEX}^L_{86} + 36.\sim\!\!7\underline{37} \quad [3]$$

$$\underline{\text{SST} = 68.4 * \text{TEX}^H_{86} + 38.6} \quad [4]$$

$$\underline{\text{SST} = 54.7 * \text{TEX}^H_{86} + 30.7} \quad [5]$$

$$\text{SLST} = 46.6 * \text{TEX}_{86} - 5.6 \quad [\sim\!\!4 6]$$

In order to assess whether the reconstruction of water temperatures using the $\text{TEX}^L_{86}/\text{TEX}^H_{86}$ is affected by ~~the~~a contribution of terrestrial-derived GDGTs, we calculated the branched isoprenoid tetraether index (BIT) (Hopmans et al., 2004):

$$\text{BIT} = ([GDGT\text{-}1] + [GDGT\text{-}2] + [GDGT\text{-}3]) / ([Crenarchaeol] + [GDGT\text{-}1] + [GDGT\text{-}2] + [GDGT\text{-}3]) \quad [\sim\!\!5 7]$$

For the analysis of long chain diols, an aliquot of each polar fraction was dissolved in DCM at a concentration of 2 mg ml^{-1} and the mixture was silylated by the addition of *N,O*-bis(trimethylsilyl)trifluoroacetamide (BSTFA) and pyridine and heating at 80 °C for 2 hours. Gas chromatography coupled to mass spectrometry (GC/MS) of long chain diols was performed using an Agilent 7890A GC coupled to an Agilent 5975B MS following the method described in Rampen et al. (2012). Long chain diols were quantified using selected ion monitoring of the masses *m/z* 313 (C_{28} 1,13- and C_{30} 1,15-diols) and *m/z* 341 (C_{30} 1,13- and C_{32} 1,15-diols). The long chain diol index (LDI) was calculated and converted to SSTs for sediments deposited in subunit Ia using the equations provided by Rampen et al. (2012):

$$\text{LDI} = [C_{30}\ 1,15\text{-diol}]/([C_{28}\ 1,13\text{-diol}] + [C_{30}\ 1,13\text{-diol}] + [C_{30}\ 1,15\text{-diol}]) \quad [\sim\!\!4 8]$$

$$\text{LDI} = 0.033 \times \text{SST} + 0.095 \quad [\sim\!\!5 9]$$

To transfer relative abundances (RA) of long chain diols found in the freshwater interval of ~~subunit Ib~~EZ1 into surface water temperatures (SWT), the lake calibration of Rampen et al. (2014) ~~has been~~was applied:

$$\text{SWT} = 26.8 - 25.9 * \text{RA } C_{28} \text{ 1,13 diol} - 54.3 * \text{RA } C_{30} \text{ 1,13 diol} + 7.4 * \text{RA } C_{30} \text{ 1,15 diol} \tag{10}$$

370

The Diol Index (DI) was calculated according to Versteegh et al. (1997):

$$\text{DI} = 100 * [C_{30} \text{ 1,15-diol}]/([C_{30} \text{ 1,15-diol}] + [C_{32} \text{ 1,15-diol}]) \tag{$\cancel{6}$11}$$

375   The methane index was determined as described by Zhang et al. (2011):

$$\text{MI} = ((([GDGT-1] + [GDGT-2] + [GDGT-3])/([GDGT-1] + [GDGT-2] + [GDGT-3] + [Crenarchaeol] + [Cren'])) \tag{12}$$

3 Results

3.1 Comparison of ^{14}C age model with palynology-based chronology

380   The ^{14}C-based age model for Site M0059 is discussed in detail by Van Helmond et al. (2017). The mean sedimentation rate was ~6.5 mm/yr and there are no obvious signs of hiatuses in Unit I. A comparison of the pollen record from Site M0059 with that of the varved high-resolution pollen record from Lake Belau in northern Germany (Dörfler et al., 2012; Figs. 1, 2), situated ~100 km south of our study site, reveals a close congruency between the pollen signals in the lacustrine and marine records. Particularly clear signals occurring in both Lake Belau and M0059 pollen records are the arrival of *Fagus* (beech) in the

385   catchment area ~6,000 cal. yr BP, a characteristic decline in *Ulmus* (elm) around ~5,600 cal. yr BP after preceding values between ~5 and ~10 %, maximum percentages of *Alnus* (alder) at ~5,200 cal. yr BP, and maximum percentages of *Fagus* between ~1,800 and ~600 cal. yr BP (Fig. 2 and Dörfler et al., 2012). Grains of cultivated Poacea taxa, i.e. cereals (Fig. 2), particularly *Triticum* (wheat) and *Secale* (rye), are consistently present after ~1,100 cal. yr BP and increase significantly after ~800 cal. yr BP. This signal is also congruent with the Lake Belau record, although the cereal pollen signal at Lake Belau is

390   stronger (Dörfler et al., 2012), probably due to higher agricultural activity close to the lake. The general palynomorph preservation is excellent over the analysed interval, and pollen concentration varies around 500,000 grains per gram sediment for most of the analysed samples. This is in accordance with the high TOC values (>2 wt%) encountered for most samples (Fig. 2). Only in the uppermost part (< 100 cal. yr BP), pollen concentration decreases to values around 200,000 grains per gram.

3.2 Pollen-based climate reconstruction

The pollen-based climate reconstructions reveal a general increasing trend from ~7,800 to ~2,000 cal. yr BP in both annual precipitation and annual temperature (TANN; Figs. 3, 4). The increase in the latter from ~5 to almost 9 °C is tied to an increase in coldest month temperatures (MTCO; ~-8 to almost 0 °C), while warmest month temperatures (MTWA) show a decreasing trend starting at ~7,000 cal. yr BP (~19 °C), which ends at ca. 2,000 cal. yr BP (~17 °C). Between ~2,000 and ~1,000 cal. yr BP, MTWA increase to >19 °C, and subsequently decrease again to <17 °C. The MTWA maximum around ~1,000 cal. yr BP is coeval with relatively low annual precipitation values (>640 mm compared to >800 mm earlier and subsequently).

3.3 Marine ecosystem changes

The Holocene record of Site M0059 was divided into four overall environmental zones (EZs; Table 2) based on statistically assessed changes in diatom assemblages (section 3.3.1) and congruent signals of other marine proxies (benthic foraminifera – section 3.3.2, ostracods – section 3.3.4, and aquatic palynomorphs – section 3.3.5). While EZ1 is characterized by freshwater conditions, EZs 2-4 indicate a brackish-marine depositional environment that persisted in the Baltic Sea during the Littorina Sea stage. EZ1 corresponds with lithological subunit Ib (49.37-53.57 mcd), while EZs 2-4 correspond with subunit Ia.

Table 2: Environmental zones of the Holocene record of Site M0059.

Zone	Depth (mcd)	Age (cal. yr BP)	Characteristics
EZ4	~6 to top	~1,000 to present	increase in brackish diatoms, *Gymnodinium* cysts, decrease in diatom abundance
EZ3	~22 to ~6	~4,100 to ~1,000	increase in diatom and *Chaetoceros* spore abundance, decreased indicators of marine influence
EZ2	~49 to ~22	~7,400 to ~4,100	increased abundance of indicators of marine influence
EZ1	~53 to ~49	~7,800 to ~7,400	high absolute/relative values of freshwater proxies

3.3.1 Diatoms

Relative abundances of salinity-based diatom assemblages, as well as absolute diatom abundance (ADA) plotted as the number of valves per gram dry weight of sediment (v/dgw), absolute abundance of *Chaetoceros* resting spores (CRS; v/dgw), and the ratio of benthic to planktonic diatoms are presented on Figure 3. The division into four environmental zones (EZ) as described above was based on salinity preference, ADA, CRS abundance, and the ratio of benthic to planktonic diatoms (B:P). These are in general agreement with signals reflected by other proxies (see below).

EZ1 (~7,800 to ~7,400 cal. yr BP) is based on three diatom samples characterized by dominance of freshwater taxa, rare CRS abundance, (average $3.2 * 10^5$), low ADA (average $2.5 * 10^7$), and low B:P (0.48). EZ2 (~7,400 to ~4,100 cal. yr BP) is defined by a distinct increase in brackish and marine species at the expense of freshwater diatoms. In addition, there is a clear increase

420   in the B:P ratio (average 4.17), ADA (average $4.65 * 10^7$) and CRS absolute abundance (average $1.0 * 10^7$). EZ2 contains both the highest B:P and the greatest range in values of B:P. EZ3 ~~(~~(~4,100 to ~1,000 cal. yr BP) shows an increase in marine, brackish-marine, and freshwater species at the expense of brackish species. The B:P ratio (average 2.65) declines some in EZ3, however ADA (average $5.1 *10^7$) and CRS absolute abundance (average $2.2 * 10^7$) are highest in this interval compared to the rest of the core. Marine and brackish-marine species increase in abundance from the base of this zone to ~1,100 cal. yr BP

425   concurrent with a decrease in brackish species. Both diatom and CRS absolute abundance increase from the base of this zone to ~1,200 cal. yr BP. B:P increases from the base of the zone to ~1,000 cal. yr BP.

EZ4 (~1,000 cal. yr BP to present) begins with an increase in brackish species. The relative abundance of marine and brackish-marine taxa, as well as B:P ratio (average 2.07) decline rather gradually throughout this interval, whereas ADA (average $2.0 *10^7$) and CRS abundance (average $5.3 * 10^6$) decline rapidly at ~1,000 cal. yr BP and remain at low levels until the core-top.

430   The significance of the differences between the four identified EZs were assessed in regards to the percent abundance of all five salinity affinities, as well as ADA, CRS abundance, and B:P. ANOVA reveals a significant difference between the means of all of these measures (Table ~~S1~~S4 in ~~Supplement~~supplement). The Tukey-Kramer pairwise test was then used to evaluate the differences between individual EZs. Statistical differences between adjacent zones, representing change through time, are reported in Table ~~S2 (Supplement~~S5 (supplement). Pairwise statistical analysis reveals significant differences between EZ1

435   and EZ2 in terms of all ecological metrics with the exception of ADA. EZ2 and EZ3 can be distinguished statistically on the basis of the percent of diatoms with a brackish affinity, which decreases from EZ2 to EZ3, as well as CRS, which increases from EZ2 to EZ3. EZ3 can be significantly distinguished from EZ4 in terms of ADA and CRS abundance, both of which decrease. Finally, EZ3 does not have a significant change in salinity with respect to EZ4, however there is a shift in the species present between these zones.

440

3.3.2 Benthic foraminiferal assemblages

Benthic foraminifera are found in sediments covering the interval since ~7,400 cal. yr BP until today. The foraminiferal assemblages comprise very few species, with *Elphidium selseyense* (formerly named *E. excavatum* forma *selseyensis;* see Darling et al., 2016) being dominant. *Elphidium incertum* is also found throughout the entire core, while all other species occur

445   only in specific intervals. In the lower part of EZ2, from ~7,400 to ~6,600 cal. yr BP, the foraminiferal assemblages are characterised by very high frequencies of *E. incertum* and, around ~6,900 cal. yr BP, relatively higher abundance of *Ammonia beccarii* (~15% compared to <1 % in samples above and below, Fig. 3). After ~6,600 cal. yr BP the relative abundance of *A.* ~~*beccarri*~~*beccarii* is strongly reduced, while *E. incertum* continues to dominate and increases in abundance until ~5,700 cal. yr

BP. During most of the interval since ~5,700 cal. yr BP (top zone EZ3 to zone EZ1), only *E. selseyense* and *E. incertum* are found consistently, with only minor, short-term occurrences of *Elphidium albiumbilicatum* and *Elphidium magellanicum* at ~5,900 cal. yr BP and ~4,850 cal. yr. BP, as well as a short-term peak of *A. beccarii* at ~3,800 cal. yr BP. The samples representing the past ~460 cal. yr BP contain no or only very few foraminifera (*E. selseyense* and a few specimens of *E. incertum* and *E. albiumbilicatum*, Fig. 3).

3.3.3 Benthic ~~foraminfer~~foraminifer isotopes and trace metal/calcium

The difference in average Mg/Ca between *E. selseyense* and *E. incertum* was not significant (1.52 vs 1.53 mmol/mol; ~~Supplement~~supplement Fig. 1S), so for the remainder only results of *E. selseyense* are included, as they are of higher resolution. Mg/Ca values decrease from 2.96 mmol/mol at ~4,000 cal. yr BP to values between 0.62 and 1.10 mmol/mol between ~2,200-800 cal. yr BP (Fig. 4). As a species-specific calibration is absent for *Elphidium* spp., we employed the Mg/Ca-temperature calibration for *Melonis barleaanum*, which has been shown to give reasonable temperatures for the Baltic Sea area (Kristjánsdóttir et al., 2007; Anjar et al., 2012). Calculated bottom water temperatures decrease from 10.9 °C at ~4,000 cal. yr BP to 0-4 °C between ~2,200 to ~800 cal. yr BP.

δ^{18}O values show an initial increase from -1.2 to 0.4 ‰ from ~7,400 to ~6,700 cal. yr BP. δ^{18}O average -0.2 ‰ for the interval ~7,400 to ~3,700 cal. yr BP and increase to an average of 0.4 ‰ afterwards, suggesting either a more gradual decrease in bottom water temperature, an increase in bottom water salinity, or both (Fig. 4, ~~supplements~~supplement Fig. S1). δ^{13}C values increase from -3.2 ‰ at ~7,000 cal. yr BP to -2 ‰ at ~5,000 to ~4,500 cal. yr BP (Fig. 3). Afterwards values oscillate around an average of -1.3 ‰, suggesting improved ventilation of the water column ~~(supplements, Table S3).~~.

3.3.4 Ostracods

Ostracod abundance was relatively low (~5 valves/30 cm^3, 23 samples barren), but preservation was good in most samples. EZ1 is entirely comprised of freshwater species. Abundant freshwater taxa *Candona* spp. and *Cytherissa lacustris* were identified in the interval between ~7,800 and ~7,400 cal. yr BP. The rest of the record contains marine and brackish-water ostracod taxa. The ostracod assemblages imply a subdivision of EZ2 (Fig. 3). EZ2a (~7,400 to ~6,800 cal. yr BP) is mainly represented with two shallow water taxa, *Palmoconcha* spp. and *Hirschmania viridis*. The abundance peak of shallow water taxa of 6 valves/30 cm^3 is observed at ~7,000 cal. yr BP. EZ2b (~6,800 to ~3,600 cal. yr BP) contains both shallow water and deeper-living taxa, with deeper-living taxa being slightly more abundant and showing two abundance peaks in this interval. In the lower part (~6,800 to ~5,600 cal. yr BP), a peak of 7 valves/30 cm^3 is observed for deeper-living taxa at ~6,500 cal. yr BP. A short interval (~5,600 to ~5,300 cal. yr BP) is barren of ostracods. The upper part of the interval, ~5,300 to ~3,600 cal. yr BP, includes a deeper-living-taxa peak of 5 valves/30 cm^3 at ~5,000 cal. yr BP. *Sarsicytheridea bradii*, *Cytheropteron*

480 *latissimum, Elofsonella concinna, Robertsonites tuberculatus*, and *Paraciprideis* sp. are the dominant taxa in this interval. These are typical representatives of Arctic/Boreal shallow water shelf faunas (Stepanova et al., 2007). Open sea environment and salinity of 14-16 and higher is expected for this group of species (Frenzel et al., 2010). Shallower water species like *Palmoconcha* spp. and *Leptocythere* spp. are the most abundant among shallow water taxa.

EZ3 (~3,600 to ~1,000 cal. yr BP) is characterized by an overall increase in abundance and predominance of shallow water
485 taxa (reaching a peak of 15 valves/30 cm^3 at ~3,500 cal. yr BP). The most abundant taxa here are the shallow water genera *Leptocythere* spp. and *Palmoconcha* spp. These taxa are present in the underlying EZ2, but become dominant here. These genera inhabit lagoons and open sea environments with salinity above 7-12. A short interval between ~2,600 and ~2,200 cal. yr BP is barren of ostracods.

Uppermost EZ1 (covering the past ~1,000 yr) is marked by a decrease in the taxonomic diversity; it is almost solely represented
490 by *Sarsicytheridea bradii*, a taxon which can be found in open sea environments and at a salinity as low as 7 (Frenzel et al., 2010).

3.3.5 Aquatic palynomorphs

Percentages of dinocysts and freshwater algae (Fig. 3) are based on the total pollen sum (thus representing a dinocyst/pollen or a freshwater algae/pollen ratio, respectively). The freshwater algae *Pediastrum* and *Botryococcus* are present in the entire
495 record, but values >3 % are only found at >7,700 cal. yr BP (Fig. 3). We have combined the dinocysts of phototrophic taxa belonging to gonyaulacoids into one group ("G-cysts"; predominately comprising *Protoceratium reticulatum*/*Operculodinium centrocarpum*, *Spiniferites* spp., and *Lingulodinium machaerophorum*), and microreticulate, gymnodinioid cysts of *Gymnodinium* in another. Cysts of heterotrophic taxa are rare and thus not depicted in Figure 3. While not all *Gymnodinium* cysts were identified to species level, most of the encountered *Gymnodinium* cysts probably belong to *G. nolleri* (referred to
500 as *Gymnodinium* cf. *nolleri* in the following). The G-cysts percentages are >3 % between ~7,800 and ~7,400 cal. yr BP (EZ1), but increase to > 5 % around ~7,400 cal. yr BP. Thereafter, values of this proxy stay rather constant at ~10 % until ~4,000 cal. yr BP (EZ 2). For the latest ~4,000 cal. yr BP, G-cysts percentages vary around 5 %, with particularly low values around 500 cal. yr BP (EZ 4). *Gymnodinium* cf. *nolleri* cysts are almost completely absent until ~7,000 cal. yr BP, increase rapidly at ~6,800 cal. yr BP, but in the following decline and are almost absent at ~4,000 cal. yr BP. A second interval of high
505 *Gymnodinium* cf. *nolleri* abundances occurs between ~3,000 and ~300 cal. yr BP, with maximum values at ~1,000 and ~200 cal. yr BP.

3.3.6 Mollusc clumped isotopes

The analysed mollusc shell fragments were assigned to the species *Abra alba, Arctica islandica, Corbula gibba*, and *Macoma balthica* (see Table ~~S4~~S6 in ~~Supplement~~supplement). The oldest analysed mollusc is from EZ2 (~6,800 cal. yr BP) and the
510 youngest analysed shell fragment from EZ4 (~140 cal. yr BP). Clumped-isotope-inferred temperatures range from ~2 °C to

~12 °C (Fig. 4). In EZ2, temperatures vary between 5°C and 11.8°C, with a majority of temperatures around ~8°C. The two temperatures obtained in EZ3 are 2.1°C and 4.8 °C, and the single temperature obtained in EZ4 is 7.7°C (Fig 4).

3.3.7 Biomarkers

515 The Diol Index shows consistently low values of 55.2±2.7 in EZ1 but rapidly increases to values of 90.5 with the establishment of brackish-marine conditions at the start of the Littorina Sea stage (Fig. 3). Thereafter, Diol Index values gradually decline and show a minimum of 54.3 around ~4,000 cal. yr BP, after which values gradually increase again until ~3,000 cal. yr BP, where they peak at 80.1. In the following, the Diol Index stays rather constant averaging 77.0±3.0 for the remainder of the record with an exception found around ~700 cal. yr BP, at which the Diol Index decreases to values as low as 61.7.

520 TEX_{86}—based SLSTs generally evidence a warming trend throughout EZ1 with temperatures increasing from 12.9 to 14.8 °C except in the uppermost sample of this interval in which a drop in temperature to 12.5 °C is observed (Fig. 4). At the transition to the marine-brackish phase of EZ2, TEX^L_{86}-inferred temperatures rapidly increase to 19.5 °C and thereafter show a gradual decline to yield minimum SSTs of ~14 °C atin the topmost part of EZ2 (~5,000 cal. yr BP). In the following, TEX^L_{86}-SSTs gradually increase and cumulate in a peak SST of 26 °C around ~1,000 cal. yr BP, after which SSTs decline again and are at

525 a minimum of 14 °C around ~300 cal. yr BP. The uppermost part of the record (<300 cal. yr BP) is characterized by increasing SSTs that maximize at 21.1 °C in the sample closest to the core top-sample.

Branched isoprenoid tetraether index values are generally high in the freshwater interval of EZ1 with an average of 0.93±0.04 (Fig. 4). With the establishment of brackish-marine conditions (base of EZ2), the branched isoprenoid tetraether index rapidly declines to values of 0.29±0.04 and shows only little variation in the organic-rich deposits of the Littorina Sea stage. Likewise,

530 values of the methane index are with an average of 0.42±0.02 comparatively high in EZ1 but at the transition to EZ2 decrease substantially to an average of 0.12±0.05 and stays low throughout the remainder of the record.

Long chain diol distributions in EZ1 yield SWTs varying from 18.5 to 21.3 °C (average 19.7±1.3 °C). At the transition to EZ2, long-chain-diol-index-based SSTs rapidly increase to a maximum of 24.3°C. Subsequently, reconstructed SSTs gradually decline and show a minimum of 15.9 °C at the transition from EZ3 to EZ4 (~1,000 cal. yr BP) that is followed by a short-lived

535 warming event with peak temperatures of 20.8 °C around ~900 cal. yr BP. A second minimum in long-chain-diol-index-based SSTs is observed between ~800 and ~400 cal. yr BP, after which temperatures again increase toand yield a value of 18.3 °C close to the core top.

4 Discussion

The complex climatic development during the Holocene in the Baltic Sea region (Björck, 2008; Zillén et al., 2008; Andrén et

540 al. 2011) enables us to compare and validate several temperature reconstruction methods, with pollen reflecting terrestrial

conditions, the long chain diol index and the TEX$_{86}$/~~TEX$^L_{86}$~~ with its different derivatives indicating changes in the surface water, and mollusc clumped isotopes and foraminiferal Mg/Ca and δ^{18}O allowing the reconstruction of bottom water conditions. Of the various salinity proxies used in this study, diatoms, cysts of phototrophic dinoflagellates, and the Diol Index mainly reflect surface water conditions, while foraminifera and ostracods indicate changes in the bottom water.

4.1 Salinity and productivity changes

All biogenic proxies indicate a phase of low salinity during **EZ1** (before ~7,400 cal. yr BP); diatom and ostracod data suggest freshwater conditions, and diatom data additionally indicate low productivity in the lowermost part of EZ1 (Fig. 3), though this is not fully consistent with relatively high TOC values in the lowermost part of EZ1 (Fig. 2) and results of Van Helmond et al. (2017). Among the aquatic palynomorphs, remains of the green algae *Pediastrum* sp. and *Botryococcus* sp., together with low occurrences of marine dinoflagellate cysts compared to pollen grains, also indicate a significant freshwater influence. Likewise, the Diol Index shows lowest values in this interval that are in the same order of magnitude reported from other lacustrine environments (Versteegh et al., 1997). Comparison with the varved pollen record from Lake Belau (Fig. 2; Dörfler et al., 2012) suggests that EZ1 is probably not older than ~9,000 cal. yr BP, as e.g. indicated by the presence of *Alnus* and *Ulmus* (~5 % each) in the lowermost samples. Our findings are thus congruent with those of Bennike and Jensen (2011) and Van Helmond et al. (2017) who suggested that during the early Holocene, a large lake developed in the southern part of the Little Belt region.

Fully marine conditions in the southern Kattegat were already established by ~9,300 cal. yr BP (Bendixen et al., 2016), but not sooner than ~8,500 to ~7,500 cal. yr BP in the central Baltic Proper (Björck, 2008). This implies that during EZ1 the Little Belt may have been connected to the Baltic Proper, but not to the Kattegat. Bennike and Jensen (2011) suggested that the transition to brackish conditions may have started at ~8,500 cal. yr BP in the Little Belt, although the oldest dated marine shell from the Little Belt is dated to ~7,700 cal. yr BP (Bennike and Jensen, 2011), consistent with our findings.

The change to more marine conditions in **EZ2** (~7,400 to ~4,100 cal. yr BP) occurred quickly, as already implied by Andrén et al. (2015b), since most proxies show a rapid decrease or disappearance of freshwater indicators (e.g. diatoms, green algae, ostracods). At the same time, the applied salinity proxies indicate a shift to more saline conditions, e.g. increasing CRS abundance, as most *Chaetoceros* requires brackish to marine conditions (Snoeijs et al., 1993-1998) and a significant rise in the Diol Index values. Maximum abundances of dinocysts of phototrophic taxa occurred in EZ2, which are coeval with abundance maxima at the southern and southeastern coast of Sweden found by Ning et al. (2015) or Yu and Berglund (2007), and in the Gotland and the Fårö Basins (Brenner, 2005; Willumsen et al., 2013).

We suggest that maxima in *Gymnodinium* cf. *nolleri* cysts between ~6,800 and ~5,200 cal. yr BP may indicate more saline conditions, though they may also be related to increased temperature (e.g. Thorsen et al., 1995; Thorsen and Dale, 1997; see below~~) and~~), evidenced here by high TEX$^L_{86}$- and long-chain-diol-index-SST in this interval. The *Gymnodinium* peak at ~6,800

cal. yr BP has to our knowledge not yet been described from the Baltic Sea and does not seem to have occurred in the Baltic Proper (Brenner, 2005; Yu and Berglund, 2007; Ning et al., 2015). Thorsen et al. (1995) and Harland and Nordberg (2011)

575 describe later *Gymnodinium* mass occurrences from the Skagerrak and the Kattegat, but sediments of equivalent age containing our *Gymnodinium* peak at ~6,800 cal. yr BP were not recovered in the framework of those studies.

Increasing content of foraminifera per gram sediment within a short interval also point to a salinity increase, as well as the near disappearance of the foraminiferal species *A. beccarii* (<1 %) at ~6,600 cal. yr BP and the relatively high frequencies of *E. incertum* until ~5,700 cal. yr BP. *Ammonia beccarii* is a euryhaline species (Murray, 2006), but it increases in frequency in

580 lower-salinity environments in the Kattegat-Baltic Sea region (e.g. Lutze, 1974; Seidenkrantz, 1993). *Elphidium incertum* is a shallow infaunal species that favours sandy substrate, in brackish, inner shelf areas (salinity >25), where it is particularly frequent just below the halocline in stratified waters (Lutze, 1974; Darling et al., 2016). Foraminiferal-δ^{18}O values are also in line with increasing salinity, increasing from -~-1.2 to ~0.4 ‰ (Fig. 3). The following drop in *E. incertum* abundance and consequent increase in *E. selseyense* in the upper part of EZ2 may potentially be ascribed to somewhat reduced bottom-water

585 salinities, as *E. selseyense* is an opportunistic species that is widespread in tidal to shelf areas with relatively large variations in temperature and salinity (Murray, 2006; Darling et al., 2016). As stable δ^{18}O values do not suggest a strong change in salinity between ~6,600 and ~3,700 cal. yr BP, the shift in benthic foraminiferal fauna may also be linked to a reduction in bottom-water oxygenation, as *E. incertum* is also reported to require relatively high oxygen concentrations (Lutze, 1974; Murray, 2006). This, however, is not corroborated by results of Van Helmond et al. (2017), who observed a significant reduction in

590 bottom-water oxygenation only at the onset of this interval.

In terms of ostracod fauna, EZ2 can be subdivided into two sub-zones, with the lower interval ~7,400 to ~6,800 cal. yr BP representing a transitional early marine stage environment with salinity above 10-14 and the second interval ~6,800 to ~3,900 cal. yr BP with salinity above 14-16. Both ostracod intervals within EZ2 reflect the onset of the Littorina Sea and the salinity increase pattern as evidenced by the highest concentration of euhaline taxa. At the same time, the transition from lower to

595 higher salinities must have been gradual, with the lower part of EZ2 containing higher numbers of shallower water meso- and polyhaline taxa decreasing upwards. This implies that bottom water salinity change was not abrupt but occurred more gradual. There was only little change in diatom-based primary productivity compared to EZ1 and likely a deepening of the photic zone or shallowing of the water column as indicated by the sharp increase in B:P. A decreasing Diol Index and possibly also decreasing *Gymnodinium* percentages during the second half of EZ2 imply slightly decreasing surface water salinity between

600 ~5,500 and ~4,100 cal. yr BP. This is also corroborated by a decrease of the marine and brackish-marine diatom assemblages, The interval represented by EZ2 (~7,400 to ~4,100 cal. yr BP) is thus characterized by brackish to marine conditions with higher salinity at the onset of the Littorina Sea stage and slowly decreasing surface water salinity afterwards, while salinity slightly increased in the bottom water. Gustafsson and Westman (2002) regard the interval between ~6,500 and ~5,000 cal. yr BP as the most marine period in the Baltic Sea in general and suggest that low precipitation could be the main cause for the

605 particularly high salinity during this interval compared to the rest of the record. While our data points to an earlier maximum in salinity (Fig._3), a connection between low precipitation and high salinity is in accordance with the generally low

precipitation values reconstructed via the MAT (<600 mm/yr excluding one sample until 4,000 cal. yr BP) for EZ2 compared to values from the late 20th century which are generally >600 mm/yr and often reach ~800 mm/yr (Omstedt et al., 1997). In EZ3 (~4,100 to ~1,000 cal. yr BP), however, high salinity seems not to be coupled with low precipitation (Fig. 3, see below).

610

At the transition between EZ2 and **EZ3** (~4,100 to ~1,000 cal. yr BP), salinity was probably lower for a short interval, as indicated by the low values of the Diol Index and a short increase in the abundance of *A. beccarii*, which appears to be a relevant signal even though it is only reflected in one sample. In EZ3, the Diol Index, diatom and benthic foraminiferal assemblages, benthic $\delta^{18}O$, and to some degree, ostracod occurrences (with particularly high values at ~3,500 cal. yr BP and

615 the complete disappearance of the very shallow water ostracod taxa) indicate another increase in both surface and bottom water salinities between ~4,100 and ~3,000 cal. yr BP. The composition of the diatom assemblages implies that EZ3 includes another particularly marine phase of the Little Belt region. Peak marine conditions, as indicated by diatom species' salinity affinities, occur from ~1,200 to ~1,000 cal. yr BP, at the transition to EZ4. This is evident in a statistically significant decrease in brackish diatom species, while the proportions of marine and brackish-marine diatom species both increase throughout this interval.

620 The Diol Index also shows high values at the transition between EZ3 and EZ4 compared to most of the record, though relatively high values were already established since ~3,000 cal. yr BP. In this case, there is no clear coupling between increased salinity and decreased precipitation, but several temperature proxies indicate high temperatures around ~1000 cal. yr BP, pointing to higher evaporation.

Environmental Zone 3 shows diatom B:P ratios which are statistically similar to EZ2, implying a deep photic zone or shallow

625 water column (supported by a peak in shallow water ostracod taxa in EZ3) and high productivity at the seafloor. In addition, this zone is characterized by particularly high primary productivity, as indicated by ADA, CRS, and somewhat increased benthic foraminifera and ostracod abundances. Also precipitation was increased, likely causing increased freshwater runoff indicated by the pollen assemblages (Fig. 3).

Following the peak marine interval, **EZ4** (since ~1,000 cal. yr BP) begins with increases in brackish diatom taxa and decreases

630 in marine and brackish-marine diatom species to the core-top. These changes between EZ3 and EZ4 imply that species shifts are more likely related to variations in primary productivity and nutrient conditions than salinity. Yet, however, the Diol Index and *Gymnodinium* percentages also decrease during this interval. In case of *Gymnodinium*, the decrease could be tied to temperature changes (according to Thorsen and Dale, 1997; see below). This might also be the case for the Diol Index as a slight correlation between this proxy and water temperature has been reported previously (Rampen et al., 2012). Productivity

635 decline from EZ3 to EZ4 is demonstrated by statistically significant decreases in ADA and CRS abundance. The uppermost diatom sample in this interval has the lowest recorded ADA as well as the lowest B:P of any brackish water interval in this study. This sample ~~(of almost recent age~~(~5 cal. yr BP) likely represents modern human influence to the Baltic Sea, i.e. eutrophication. Eutrophication would cause a decline in overall diatom abundance, as diatoms are often replaced by cyanobacteria (O'Neil et al., 2012; Michalak et al., 2013) and dinoflagellates (Wasmund and Uhlig, 2003) in cases of high

640 levels of nutrient loading. In turn, this would lead to a shallowing of the photic zone resulting from sunlight being rapidly

absorbed by cyanobacteria and dinoflagellates in the upper water column, as seen in the low B:P ratio. The relative and absolute amount of dinocysts is decreasing though in the uppermost palynology sample, thus denser sampling will be needed to determine the anthropogenic impact to the Baltic Sea ecosystems in future studies. Human influence is, however, indicated by the significant increase of pollen of cultivated Poacea taxa (Fig. 2), starting at ~1,000 cal. yr BP, with persistent occurrences since ~700 cal. yr BP. The coeval decrease of pollen of tree taxa like *Alnus* and *Fagus* may be an anthropogenic deforestation signal due to increased agricultural activity (Fig. 2).

The *Gymnodinium* maxima encountered in EZ3 and EZ4 are probably temporally related to two mass occurrences of *Gymnodinium* in the eastern Kattegat as described by Harland and Nordberg (2011) for ~2,000 and ~300 cal. yr BP. The occurrence of *Gymnodinium* cysts in the sediments from the Skagerrak/Kattegat is tied to warm water conditions according to Thorsen and Dale (1997). This connection would be congruent with our findings that the maximum at the transition from EZ3 to EZ4 is coeval with the Medieval Warm Period (MWP, also called the Medieval Climate Anomaly) and with high/increasing temperatures. However, while Thorsen and Dale (1997) assign the cysts to *G. catenatum*, Harland and Nordberg (2011) claim that the *Gymnodinium* cysts found in Holocene sediments from the Skagerrak and Kattegat rather belong to *G. nolleri* (in accordance with our results) and that the known mass occurrences may not be tied to high temperatures. Considering our findings, *Gymnodinium* mass occurrences may as well be tied to particularly high salinity as implied by the good correlation with other salinity proxies, e.g. the Diol Index (which varies around values of ~80, Fig. 3), but higher resolution studies beyond the scope of this study would be needed to be able to prove such a connection statistically. EZ4 is characterized by a taxonomic diversity decrease in ostracods; this assemblage is almost solely represented by one species, *S. bradii*. This change may imply an unfavourable habitat for ostracods probably related to shallowing of the site and low oxygen conditions.

Taken together, the different salinity proxies provide a consistent picture of how salinity in the water column changed in the Little Belt during the last ~8,000 cal. yr BP with freshwater conditions preceding ~7,400 cal. yr BP and more saline conditions thereafter. Precipitation (reconstructed via pollen assemblages) may have been one of the factors influencing salinity, particularly between ~8,000 and ~4,000 cal. yr BP. Slight discrepancies between the salinity proxies are likely explained by a(i) differences between surface and bottom waters and b(ii) other factors influencing microfossil assemblages such as productivity and temperature. While qualitative estimates are congruent for most proxies, quantitative salinity estimates could rarely be made in the framework of ourthis study.

4.2 Temperature reconstructions

Inorganic- (e.g. Mg/Ca and $\delta^{18}O$ of benthic foraminifera, clumped isotopes) and organic-based temperature proxies (e.g. TEX_{86}, long chain diol index) have become indispensable tools in paleoenvironmental research as they provide quantitative information of past climate variations. Yet, proxy-based temperature estimates may vary significantly and/or show different trends even within the same sample set. This apparent mismatch between proxies severely complicates their application in

paleoenvironmental and -climate research. Ideally, multiple proxies should therefore be used simultaneously to provide independent paleotemperature records (e.g. ~~Krossa~~Butruille et al., 2017; Jonas et al., 2017).

675 Pollen-based reconstruction of seasonal and mean annual air temperatures as well as estimates on surface water temperature variations using lipid paleothermometers ~~are~~ were obtained ~~for~~continuously over the ~~entire~~investigated sequence of Site M0059, but clumped isotope and Mg/Ca data are missing in particular from the freshwater interval reflected in **EZ1** and in the lowermost section of EZ2 due to the lack of sufficient carbonaceous micro- and macrofossils. Despite the low resolution of some ~~proxies~~of the investigated parameters, there is a certain degree of similarity in temperature trends observed across the different proxies ~~used in this study~~. The pollen-based temperatures reconstructed for the two uppermost samples from the

680 interval between 100 cal. yr BP and the present show an average value of ~0.1 °C for MTCO and of ~16.4 °C for MTWA, which is close to ~~with~~ mean temperatures observed in Denmark during January (~1.5 °C) and August (~17.2 °C; Danish Meteorological Institute, 2017). The most complete temperature records are provided by the sedimentary distribution of isoprenoid GDGTs (TEX$_{86}$ and its derivatives) and long chain diols (in form of the long chain diol index).

Although absolute temperature estimates differ between the two proxies, trends are overall very similar in freshwater interval

685 EZ1 showing a rather constant SWT of 13.5±1.0 °C (TEX$^L_{86}$) and 19.7±1.3 °C (long chain diols), followed by a rapid temperature increase in both lipid paleothermometers to maximum values of 19.5 °C (TEX$^L_{86}$) and 24.5 °C (long chain diol index) at the transition from EZ1 to **EZ2** at ~7,400 cal. yr BP (Fig. 4). An interval of generally higher mean annual air and water temperatures has previously been described from other records of the Baltic Sea region such as Lake Flarken, Sweden (Seppä et al., 2005) or the Skagerrak (Butruille et al., 2017; Krossa et al., 2017) and is consistent with the Holocene Climate

690 Optimum (HCO~~), a time period of warm summers in higher latitudes.~~, also Holocene Thermal Maximum, e.g. Seppä et al., 2005). The pollen-based temperature reconstructions imply that in the terrestrial realm, high summer temperatures were already established before ~7,400 cal. yr BP, but that temperatures were very low during winter. In EZ2, the MTWA and SWTs based on the long chain diol index indicate a gradual and slow cooling trend by ~1 to 4 °C towards the top of EZ2. A similar cooling trend is also observed in the TEX$^L_{86}$ record that despite generally high surface water temperatures shows a

695 decline in temperature by ~6 °C during EZ2. The general order of magnitude of the pollen-based temperatures for EZ2 (~-8 to ~1.5°C MTCO and ~19 to ~17.5°C MTWA) is in accordance with pollen-based climate reconstructions from, e.g.~~.~~, central Germany (Kühl and Moschen, 2012). Furthermore, the overall trends in all temperature reconstructions are congruent with trends reported by Davis et al. (2003) and Mauri et al. (2015) for western central/northern Europe~~.~~ based on pollen records. However, ~~findings~~the presence of pollen of thermophilous species in Danish records from the Boreal and the Atlantic

700 ~~periods~~period (~9,000 to 5,000 cal. yr BP) imply that winters ~~should~~ have been mild enough for these taxa (e.g. Iversen, 1944).

In **EZ3**, the long- chain- diol- index-based ~~SST~~ SSTs, pollen-inferred MTWA and Mg/Ca ratios suggest a continuation of the cooling that agrees with trends observed in other records (Seppä et al., 2005), while MTCO, TANN and the TEX$^L_{86}$ indicate a gradual warming that cumulates in maximum air and surface water temperatures at the transition to EZ4 at ~1,000 cal. yr BP

and therewith in a time interval equivalent to the Medieval Warm Period (MWP). A congruent short-lived warming that interrupts the general cooling trend is also observed in the long chain diol index-inferred temperature record.

In **EZ4**, the long- chain- diol- index- and TEX$^L_{86}$-based SSTs show a rapid cooling with minimum temperatures of 14°C (TEX$^L_{86}$) and 17°C (long chain diol index) observed at ~400 cal. yr BP. Such a cooling trend is also evident in all pollen-based temperature reconstructions and likely corresponds to the Little Ice Age (LIA). In contrast to the pollen record, however, the long chain diol index and TEX$^L_{86}$ both show a warming trend in the uppermost part of the studied sequence with SSTs ~~exceeding~~close to 20 °C in the sample closest to the core top. Surface water temperatures of similar magnitude are presently observed during late July to mid-August in the Little Belt (ICES, 2017) and imply that both lipid paleothermometers reflect a late summer signal in our setting. For the TEX$^L_{86}$, this finding is in agreement with previous observation made by Kabel et al. (2010) in the Baltic Proper. Likewise, the long chain diol index has been reported to reflect summer surface water temperatures in a variety of oceanographic regions (Lopes dos Santos et al., 2013; Jonas et al., 2017), although it has recently been advocated to reflect an annual water temperature signal in the Ångermanälven River estuary (Warnock et al., 2017).

Reconstructed absolute temperatures vary significantly between the different inorganic ~~based~~ and organic-based proxies (Fig. 4). This is ~~–~~ to some extent ~~–~~ explained by the different realms the proxies reflect but even between the long chain diol index and TEX$^L_{86}$ ~~lipid paleothermometers~~, which are both considered to reflect summer ~~SSTs~~SWTs in the Baltic Sea, significant deviations are observed. Such discrepancies have previously been reported for both proxies from subpolar (Rodrigo-Gámiz et al., 2015) to tropical regions (Jonas et al., 2017) and were explained by differences in either the habitat depth and/or seasonality of the biological sources of both proxies. Long chain diols used to calculate the long chain diol index are synthesized by eustigmatophyte algae (Volkman et al., 1992~~) that~~), which are oxygenic photoautotrophs~~,~~ and therefore ~~the long chain diol index~~this organic temperature proxy should exclusively record SWTs. Indeed, the long- chain- diol- index-based SWT in the sample closest to the core top is 18.3°C and therewith closely matches the summer ~~SST~~SWT of 17.6±0.7°C observed in the Little Belt region (ICES, 2017). This finding is in accordance with the observation that the long chain diol index reflects ~~SST during~~ the late summer-autumn season water temperature based on a comparison of long chain diol distribution patterns in globally distributed marine surface sediments and monthly satellite SST data (Rampen et al., 2012). In addition to the marine realm, long chain diols ~~have~~are also ~~been observed~~ubiquitously found in freshwater environments ~~(.~~ Rampen et al~~.,~~. (2014~~).~~ ~~These authors)~~ noted a ~~moderate~~strong linear correlation between ~~summer temperatures and~~ the distribution of long chain ~~diol index~~diols in a set of globally distributed lake sediments. ~~Yet, the slope of long chain diol index regression lines found in lacustrine and marine settings differs significantly, suggesting that~~ and annual mean as well as summer surface water temperatures, possibly allowing the reconstruction of ~~long chain diol index-based SWT may be flawed in settings of high~~ past continental temperature changes from lacustrine systems. Yet, the riverine ~~input~~transport of such freshwater-derived long chain diols to marine environments may confound the robust application of ~~organic matter.~~the LDI in coastal systems as long chain diol distribution patterns in lacustrine and marine settings show different response to temperature. Indeed, substantial offsets between long- chain- diol- index-based SSTs and satellite derived SSTs have been observed in front of the Tagus and Sado

river mouths (Iberian Atlantic margin) with the long chain diol index yielding ~~SST~~temperatures that are up to 8 °C lower than measured average or summer SSTs (de Bar et al., 2016). ~~Yet~~In our setting, the branched isoprenoid tetraether index, a relative measure for the loading of terrestrial organic matter to aquatic environments (Hopmans et al. 2004), is characterized by consistently low values in brackish-marine EZ2-4 that ~~speak~~point against an increased freshwater discharge that may have confounded the use of the long chain diol index ~~in our setting.~~(see below).

Temperatures reconstructed using the ~~sedimentary distribution of isoprenoid GDGTs (i.e, TEX₈₆/~~TEX$^L_{86}$~~)~~ vary from ~12 to ~26 °C (average of 17.0±3.5 °C) with three distinct maxima observed at the base of EZ2 (~7,500 to ~7,300 cal. yr BP; 19.6±0.1 °C) as well as in the lowermost part of EZ4 (~900 cal. yr BP; 25.9 °C) and close to the core top ~~of EZ4~~ (16 cal. yr BP; 21.1°C). The latter ~~present day~~ TEX$^L_{86}$–based water temperature is close to ~~SSTs~~SWTs observed in the Little Belt region during late July to mid-August (ICES, 2017). This suggests that the TEX$^L_{86}$ ~~reflects~~, similar to the long chain diol index, may reflect summer surface water temperatures in the Baltic Sea as previously also argued by Kabel et al. (2012), who observed the best correlation for isoprenoid GDGT distribution patterns in surface sediments of the central Baltic with average water temperatures from July to October. ~~The~~ The TEX$^H_{86}$ has also been shown to correlate best with summer surface water temperatures in the Baltic Sea but correlations between this proxy and water temperatures are less strong as compared to those derived from the TEX$^L_{86}$ (Kabel et al~~.~~., 2012). Yet, the TEX$^H_{86}$-reconstructed temperature for the sediment closest to the core top is 18.9 °C and therewith it is closer to the average summer SWT of 17.6±0.7°C measured in the modern Little Belt. In addition, absolute temperatures inferred from the TEX$^H_{86}$ are generally lower, ranging from 12.6 to 20.6 °C, and thereby show a significantly smaller amplitude compared to those derived from the TEX$^L_{86}$. The calculation of this proxy, however, requires the robust identification of the crenarchaeol regioisomer that in ~~the~~ marine ~~environment~~environments is ubiquitously distributed ~~(Schouten et al., 2002). In~~ but in brackish and freshwater ~~environments this component~~systems is generally less abundant (e.g. Schouten et al., 2013b~~) and in~~). In the Little Belt ~~region~~, it could ~~not~~ be detected ~~in all the samples and generally~~ with ~~less~~only little confidence in ~~the remaining~~most samples ~~questioning the use of the TEX$^H_{86}$~~, resulting in ~~reconstructing SWTs~~comparatively high scatter with several abrupt temperature shifts by 5 °C or higher in TEX$^H_{86}$- reconstructed SSTs. Therefore, the reconstruction of water temperatures based on the TEX$^H_{86}$ seems to be less robust compared to the TEX$^L_{86}$ in the Baltic Sea. ~~A factor~~Molecular analysis evidences that thaumarchaeotal abundance in the central Baltic Sea is highest at greater water depth associated with increased rates of nitrification in oxygen-deficient bottom waters (Berg et al., 2014). As isoprenoid GDGTs may thus also derive from deeper parts of the water column, we also calculated subsurface water temperatures using the calibration of Kim et al. (2012). Reconstructed temperatures varied from 9.0 to 16.3 °C (average 12.7±1.7 °C) and therewith significantly exceeded average (7.6±0.6 °C) as well as summer bottom water temperatures (9.3±1.3 °C) in the Little Belt region (Fig. 5). It thus seems unlikely that deep water-dwelling Thaumarchaeota constitute a major source of isoprenoid GDGTs at our site. Hence, in contrast to some recent studies that have argued for the TEX$_{86}$ and its derivatives to specifically record water temperatures at the depth of e.g. the thermocline (Lopes dos Santos et al., 2013; Jonas et al., 2017), the TEX$^L_{86}$ at least in the western Baltic Sea may reflect a surface water temperature signal. Other factors potentially complicating the reconstruction of ~~GDGT~~TEX$^L_{86}$-based SWTs is the input of large quantities of soil-derived isoprenoid

GDGTs (Weijers et al., 2006; Schouten et al., 2013b~~).~~) or admixtures of high abundances of GDGT derived from sedimentary Euryarchaeota involved in the anaerobic oxidation of methane (AOM; Weijers et al. 2011). A larger contribution of isoprenoid GDGTs synthesized by methanotrophic archaea can be excluded for our site as the methane index, a quantitative ~~mean~~measure for the relative contribution of GDGTs derived from AOM-related archaea to the total GDGT pool (Zhang et al., 2011), generally does not exceed a value of 0.2 and thus argues against a strong impact of methanotrophic archaea in the brackish-marine sediments of EZ2-4 (Fig. 5). In order to determine the input of terrestrial organic matter to ~~aquatic environments is~~the Little Belt region, we employed the branched isoprenoid tetraether index ~~with~~. In aquatic environments, low values of this proxy (<0.1) ~~indicating~~indicate open marine conditions ~~and~~, while high values ~~being~~are more representative for terrestrial settings (<0.9; Hopmans et al., 2004). Empirical studies suggest that the TEX_{86} and its derivatives do not allow a reliable reconstruction of ~~SSTs~~SWTs if branched isoprenoid tetraether index values exceed a threshold of ~0.3 (Weijers et al., 2006; Zhu et al., 2011). Branched isoprenoid tetraether index values in the Little Belt have an average of 0.29±0.04 in EZ2-4, close to but still below this threshold. The TEX^{L}_{86} does, therefore, not seem to be biased by ~~an~~large allochthonous ~~contribution~~contributions of isoprenoid GDGTs. This is also supported by an absence of correlation between the branched isoprenoid tetraether index and TEX^{L}_{86} values ($r^2 = 0.04$; p >0.001), which is only to be expected if the terrestrial influence on the TEX^{L}_{86} is negligible (Schouten et al., 2013a). In fact, a TEX^{L}_{86} temperature record with similar trends, covering only the last 1,000 cal. yr BP with temperature maxima during the MWP and the Modern Hypoxic Period, has been reported from the Gotland Basin in the central Baltic Proper (Kabel et al., 2012), suggesting that the TEX^{L}_{86} indeed traces climate-driven variations in SWT in the brackish-marine Littorina Sea stage.

Temperatures inferred from carbonate-clumped isotopes and Mg/Ca ratios of benthic foraminifera are largely similar to those observed during late summer in the Little Belt. Indeed, in temperate climate settings molluscs and benthic foraminifera precipitate carbonate only if environmental conditions permit, so shell geochemical proxies (such as carbonate clumped isotopes and Mg/Ca) tend to be skewed towards the seasons when growth is favourable (Filipsson et al., 2004; Austin et al., 2006; Schöne, 2008; Skirbekk et al., 2016). Despite temperatures, which are within range of present day variability, the cleaning experiments on the foraminiferal calcite show that the 8°C decrease in bottom water temperatures may not be realistic after all. It cannot be excluded that the foraminiferal tests were still contaminated by the presence of authigenic carbonates like for example rhodochrosite, which can also contain Mg, and which cannot be removed by the current cleaning methodologies. The occurrence of such authigenic carbonate deposits in the Baltic Sea is common (Huckriede and Meischner, 1996; Andrén et al., 2015b; Hardisty et al., 2016; Van Helmond et al., 2017) and likely also affects foraminiferal tests (Groeneveld and Filipsson, 2013). Remaining contamination is also suggested by the significant correlation coefficient between Mg/Ca and Mn/Ca ($r^2 = 0.72$) after the oxidation-reduction cleaning. This suggests that especially the older part of the Mg/Ca record, where both Mg/Ca and Mn/Ca display highest ratios, is contaminated.

The presence of benthic foraminifera in EZ2-4 and their absence in EZ1 is related to salinity, i.e. foraminifera ~~do~~did not occur in the freshwater setting of EZ1. The absence of foraminifera in the upper meters of the record (<5 mcd), however, is more likely due to poor preservation of the foraminiferal calcite. Similarly, the foraminiferal abundance ~~decreases~~decreased in EZ2,

such that enough specimens were ~~still~~ present to perform stable ~~isotopes~~isotope analyses, but there were too few to perform reliable Mg/Ca analyses. Poor preservation may have been caused by the degradation of organic matter in the sediment, which led to lower pH values of the pore water such that dissolution of the foraminiferal tests took place.

5 Conclusions

In this study, we have investigated and compared how inorganic- and organic-based temperature as well as salinity proxies perform in the coastal setting of the Little Belt with highly variable environmental conditions. Sediments deposited since ~7,800 cal. yr BP at IODP Site M0059 were analysed to capture the transition from freshwater to marine conditions and thus to study the effect of facies change on proxy applications.

Our study demonstrates that a multi-proxy approach allows deciphering the various factors which have influenced past oceanographic conditions in the Little Belt. Between ~7,800 and 7,400 cal. yr BP, a direct connection of the Little Belt to the Baltic Proper may have existed as salinity-specific proxies indicate lacustrine conditions, while a connection to the Kattegat can be excluded. Salinities and probably also water temperatures increased within 200 yr after the onset of the Littorina Sea stage at ~7,400 cal. yr BP. An interval of particularly saline conditions and high summer water and air temperatures followed, although both salinity and water temperatures declined with increasing precipitation until ~4,000 cal. yr BP. After ~4,000 cal. yr BP, the Little Belt witnessed decreasing temperatures during the warm season both in the marine and terrestrial realm, while salinity increased.

In addition, our study highlights the importance and value of a multi-proxy approach to reconstruct past oceanographic conditions. The different salinity proxies used here show generally similar trends in relative changes in salinity, but do not allow quantitative estimates of salinity (except for marine ostracods). In contrast, the reconstruction of temperatures is associated with particularly large uncertainties and variations in absolute values by up to 8 °C for bottom waters and even up to 16 °C for summer surface waters. For example, different cleaning techniques for Mg/Ca in the foraminifera show different results which partly correlate with indicators for contamination especially in the deeper intervals studied. This suggests that the Mg/Ca of those samples is likely over-estimated, so that the decreasing trend in Mg/Ca and thus calculated bottom water temperatures may not be as large. The differences in results based on the lipid proxies (long chain diol index and TEX^L_{86}) can partly be explained with the application of modern-day proxy calibrations in areas which experienced significant changes in depositional settings (e.g. change from freshwater to marine conditions). Our study shows that particular caution has to be taken when applying and interpreting proxies in coastal environments, where water mass conditions can experience more rapid and larger changes than in open-ocean settings. Approaches using a multitude of independent proxies may thus allow more robust paleoenvironmental assessment.

6 Data availability

Data not enclosed in the ~~supplements~~supplement will be uploaded to the PANGEA database (LINK). ~~Already available are~~All ostracod data is accessible via PANGEA (PDI-14486).

840

Acknowledgements.

This investigation used samples from IODP Expedition 347, and we are very grateful to IODP and ESSAC for funding and organising the expedition. Stephen Obrochta, Sofia Ribeiro, Ingo Feeser, and Walter Doerfler are gratefully acknowledged for insightful discussions and comments on the age model, dinoflagellate cyst taxonomy and ecology, and the Lake Belau pollen

845 record. We thank the crew and science party of IODP Expedition 347 as well as the technical staff at MARUM, Bremen, for their support during the expedition's off- and onshore phases. We are grateful for technical support from the different laboratories involved in the study. We thank Audrey Limoges, Filipa Naughton, and an anonymous referee for their detailed input to the discussion paper, and we thank Markus Kienast for editing. This research was supported by the German Research Foundation (grants KO3944/6-1 to UK, and BA3841/5-1 to TB), the Carlsberg Foundation and Geocenter Denmark (grants to

850 MSS and ORC), and US National Science Foundation (NSF grant #T347A13). TA, JG, NQK, and HLF thank the Swedish research councils VR and FORMAS, the LAM Foundation, the Crafoord Foundation as well as the Center for Environmental and Climate Research at Lund University for funding. TA and EA acknowledge funding from The Foundation for Baltic and East European Studies (grants 1562/3.1.1/2013 and 2207/3.1.1/2014). JLA was supported by the National Science Foundation (NSF-DGE-1144087 and OCE-0652315). CPS and NVH acknowledge funding from the European Research Council (ERC

855 Starting Grant 278364) and the Netherlands Organisation for Scientific Research (NWO-Vici 865.13.005)

Edited by: Markus Kienast

860 Reviewed by: Audrey Limoges, Filipa Naughton, and an anonymous reviewer.

References

Andrén, E., Andrén, T., and Kunzendorf, H.: Holocene history of the Baltic Sea as a background for assessing records of human impact in the sediments of the Gotland Basin. The Holocene, 10, 687-702, https://doi.org/10.1191/09596830094944, 2000.

865 Andrén, T., Björck, S., Andrén, E., Conley, D., Zillén, L., and Anjar, J.: The development of the Baltic Sea basin during the last 130 ka, in: The Baltic Sea Basin, Harff, J., Björck, S., and Hoth, P. (eds.), Springer, Berlin, 75–97, 2011.

Andrén, T., Jørgensen, B.B., Cotterill, C., and the Expedition 347 Scientists: Baltic Sea Paleoenvironment. Proceedings IODP, 347. College Station, TX (Integrated Ocean Drilling Program), https://doi.org/10.2204/iodp.proc.347.101.2015, 2015a.

Andrén, T., Jørgensen, B.B., Cotteril, C., Green, S., and the IODP expedition 347 scientific party: Baltic Sea basin
870   paleoenvironment and biosphere. Scientific Drilling, 20, 1-12, https://doi.org/10.5194/sd-20-1-2015, 2015b.

Anjar, J., Adrielsson, L., Bennike, O., Björck, S., Filipsson, H.L., Groeneveld, J., Knudsen, K.L., Larsen, N.K., and Möller, P.: Palaeoenvironmental history of the Baltic Sea basin during Marine Isotope Stage 3. Quat. Sci. Rev., 34, 81-92, https://doi.org/10.1016/j.quascirev.2011.12.009, 2012.

Austin, W.E.N., Cage, A.G., and Scourse, J.D.: Mid-latitude shelf seas: a NW European perspective on the seasonal dynamics
875   of temperature, salinity, and oxygen isotopes. The Holocene, 16, 937-947, https://doi.org/10.1177/0959683606hl985rp, 2006.

Barker, S., Greaves, M., and Elderfield, H.,: A study of cleaning procedures used for foraminiferal Mg/Ca paleothermometry. Geochem., Geophys., Geosys., 4, https://doi.org/10.1029/2003GC000559, 2003.

Bendixen, C., Jensen, J.B., Boldreel, L.O., Clausen, O.R., Bennike, O., Seidenkrantz, M.-S., Nyberg J., and Hübscher, C.: The Holocene Great Belt connection to the southern Kattegat, Scandinavia: Ancylus Lake drainage and Early Littorina Sea
880   transgression. Boreas, 46, 53-68, https://doi.org/10.1111/bor.12154, 2016.

Bennike, O. and Jensen, J.B.: Postglacial, relative shore-level changes in Lillebælt, Denmark. Geol. Surv. Den. Green. Bull., 23, 37–40, 2011.

Berg, C., Vandieken, V., Thamdrup, B., and Jürgens, K.: Significance of archaeal nitrification in hypoxic waters oft he Baltic Sea. ISME J., 9, 1319-1332, 2015.

885   Björck, S.: The late quaternary development of the Baltic Sea Basin, in: Assessment of Climate Change for the Baltic Sea Basin, The BACC Author Team (eds.), Springer-Verlag, Berlin-Heidelberg, 398–407, 2008.

Björck, S., Andrén, T., and Jensen, J.B.: An attempt to resolve the partly conflicting data and ideas on the Ancylus-Littorina transition. Polish Geological Institute Special Papers 23, 21-25, 2008.

Blaauw, M.: Methods and code for 'classical' age-modelling of radiocarbon sequences. Quat. Geochronol., 5, 5512-5518,
890   https://doi.org/10.1016/j.quageo.2010.01.002, 2010.

Bordon, A., Peyron, O., Lézine, A.-M., Brewer, S., and Fouache, E.: Pollen-inferred Late-Glacial and Holocene climate in southern Balkans (Lake Maliq). Quatern. Int., 200, 19-30, https://doi.org/10.1016/j.quaint.2008.05.014, 2009.

Brenner, W.W.: Holocene environmental history of the Gotland Basin (Baltic Sea) – a micropalaeontological model. Palaeogeogr. Palaeocl., 220, 227–241, https://doi.org/10.1016/j.palaeo.2004.12.010, 2005.

895   Butruille, C., Krossa, V.R., Schwab, C., and Weinelt, M.: Reconstruction of mid- to late-Holocene winter temperatures in the Skagerrak region using benthic foraminiferal Mg/Ca and δ^{18}O. The Holocene, 1, 63-721-10, https://doi.org/10.1177/0959683616652701, 2017.

Conley, D.J., Carstensen, J., Aigars, J., Axe, P., Bonsdorff, E., Eremina, T., Haahti, B.-M., Humborg, C., Jonsson, P., Kotta, J., Lännegren, C., Larsson, U., Maximov, A., Medina, M.R., Lysiak-Pastuszak, E., Remeikaite-Nikiene, N., Walve, J.,

900   Wilhelms, S., and Zillén, L.: Hypoxia is increasing in the coastal zone of the Baltic Sea. Envir. Sci. Tech., 45, 6777-6783, https://doi.org/10.1021/es201212r, 2011.

Danish Meteorological Institute: http://www.dmi.dk/vejr/arkiver/normaler-og-ekstremer/klimanormaler-dk/vejrnormal/ visited 24.02.2017.

Darling, K.D., Schweizer, M., Knudsen, K.L., Evans, K.M., Bird, C., Roberts, A., Filipsson, H.L., Kim, J.-H., Gudmundsson,

905   G., Wade, C.M., Sayer, M.D.J., and Austin, W.E.N.: The genetic diversity, phylogeography and morphology of Elphidiidae (Foraminifera) in the Northeast Atlantic. Mar. Micropalaeontol., https://doi.org/10.1016/j.marmicro.2016.09.001, 2016.

Castañeda I.S. and Schouten, S.: A review of molecular organic proxies for examineing modern and ancient lacustrine environments. Quaternary Sci. Rev., 30, 2851-2891, https://doi.org/10.1016/j.quascirev.2011.07.009, 2011.

Davis, B.A.S., Brewer, S., Stevenson, A.C., Guiot, J., and Data Contributors: The temperature of Europe during the Holocene

910   reconstructed from pollen data. Quaternary Sci. Rev. 22, 1701-1716, https://doi.org/10.1016/S0277-3791(03)00173-2, 2003.

de Bar, M.W., Dorhout, D.J.C., Hopmans, E.C., Rampen, S.W., Sinninghe Damsté, J.S., and Schouten S.: Constraints on the application of long chain diol proxies in the Iberian Atlantic margin. Org. Geochem., 101, 184-195, https://doi.org/10.1016/j.orggeochem.2016.09.005, 2016.

Dennis, K.J., Affek, H.P., Passey, B.H., Schrag, D.P., and Eiler, J.M.: Defining an absolute reference frame for 'clumped'

915   isotope studies of CO_2. Geochim. Cosmochim. Ac., 75, 7117-7131, https://doi.org/10.1016/j.gca.2011.09.025, 2011.

Diaz, R. J. and Rosenberg, R.: Spreading dead zones and consequences for marine ecosystems. Science, 321, https://doi.org/10.1126/science.1156401, 2008.

Dörfler, W., Feeser, I., van den Bogaard, C., Dreibrodt, S., Erlenkeuser, H., Kleinmann, A., Merkt, J., and Wiethold, J.: A high-quality annually laminated sequence from Lake Belau, Northern Germany: Revised chronology and its implication for

920   palynological and tephrochronological studies. The Holocene 22(12), 1413–1426, https://doi.org/10.1177/0959683612449756, 2012.

Dormoy, I., Peyron, O., Combourieu Nebout, N., Goring, S., Kotthoff, U., Magny, M., and Pross, J.: Terrestrial climate variability and seasonality changes in the Mediterranean region between 15 000 and 4000 years BP deduced from marine pollen records. Clim. Past 5, 615-632, https://doi.org/10.5194/cp-5-615-2009, 2009.

925   Eiler, J.M.: Paleoclimate reconstruction using carbonate clumped isotope thermometry. Quaternary Sci. Rev., 30, 3575-3588, https://doi.org/10.1016/j.quascirev.2011.09.001, 2011.

Ezat, M.M., Rasmussen, T.L., and Groeneveld, J.: Reconstruction of hydrographic changes in the southern Norwegian Sea during the past 135 kyr and the impact of different foraminiferal Mg/Ca cleaning protocols. Geochem., Geophys., Geosyst., 17, https://doi.org/10.1002/2016GC006325, 2016.

930   Filipsson, H.L. and Nordberg, K.: Climate Variations, an overlooked Factor influencing the Recent Marine Environment. An Example from Gullmar Fjord, Sweden, Illustrated ny Benthic Foaminifera and Hydrographic Data. Estuariues, 27, 867-881, https://doi.org/10.1007/BF02912048, 2004

Filipsson, H.L., Nordberg, K., and Gustafsson, M.: Seasonal study of $\delta^{18}O$ and $\delta^{13}C$ in living (stained) benthic foraminifera from two Swedish fjords. Mar. Micropaleontol., 53, 159-172, https://doi.org/10.1016/j.marmicro.2004.05.008, 2004.

935   Filipsson, H.L., McCorkle, D.C., Mackensen, A., Bernhard, J.M., Andersson, L.S., Naustvoll, L.-J., Caballero-Alfonso, A.M., Nordberg, K., and Danielssen, D.S.: Seasonal variability of stable carbon isotopes ($\delta^{13}C_{DIC}$) in the Skagerrak and the Baltic Sea: Distinguishing between mixing and biological productivity. Palaeogeogr. Palaeocl., in press, https://doi.org/10.1016/j.palaeo.2016.11.031, 2016.

Frenzel, P. and Boomer, I.: The use of ostracods from marginal marine, brackish waters as bioindicators of modern and
940   Quaternary environmental change. Palaeogeogr. Palaeocl., 225, 68-92, https://doi.org/10.1016/j.palaeo.2004.02.051, 2005.

Frenzel, P., Keyser, D., and Viehberg, F.A.: An illustrated key and (palaeo)ecological primer for postglacial to Recent Ostracoda (Crustacea) of the Baltic Sea. Boreas, 39(3), 567–575, https://doi.org/10.1111/j.1502-3885.2009.00135.x, 2010.

Greaves, M., Caillon, N., Rebaubier, H., et al.: Interlaboratory comparison study of calibration standards for foraminiferal Mg/Ca thermometry. Geochem., Geophys., Geosyst., 9, Q08010, https://doi.org/10.1029/2008GC001974, 2008.

945   Groeneveld, J. and Filipsson, H.L.: Mg/Ca and Mn/Ca ratios in benthic foraminifera: the potential to reconstruct past variations in temperature and hypoxia in shelf regions. Biogeosciences 10, 5125-5138, https://doi.org/10.5194/bg-10-5125-2013, 2013.

Guiot, J.: Methodology of palaeoclimatic reconstruction from pollen in France: Palaeogeogr. Palaeocl. 80, 49-69, https://doi.org/10.1016/0031-0182(90)90033-4, 1990.

Gustafsson, M. and Nordberg, K.: Living (stained) benthic foraminifera and their response to the seasonal hydrographic cycle,
950   periodic hypoxia and to primary production in the Havstens Fjord on the Swedish west coast. Estuar. Coast Shelf S., 51, 743-761, https://doi.org/10.1006/ecss.2000.0695, 2000.

Gustafsson, B.G. and Westman, P.: On the causes for salinity variations in the Baltic Sea during the last 8500 years. Paleoceanography, 17, https://doi.org/10.1029/2000PA000572, 2002.

Gustafsson, B.G., Schenk, F., Blenckner, T., Eilola, K., Meier, H.E.M., Müller-Karulis, B., Neumann, T., Ruoho-Airola, T.,
955   Savchuk, O.P., and Zorita, E.: Reconstructing the development of Baltic Sea eutrophication 1850–2006. Ambio, 41, 534-548. https://doi.org/10.1007/s13280-012-0318-x, 2012.

Hammer, Ø., Harper, D.A.T. and Ryan, P.D.: PAST: Paleontological statistics software package for education and data analysis. Palaeontol. Electron., 4, 2001.

Hardisty, D.S., Riedinger, N., Planavsky, N.J., Asael, D., Andrén, T., Jørgensen, B.B., Lyons, T.W.: A Holocene history of
960   dynamic water column redox conditions in the Landsort Deep, Baltic Sea. Am. J. Sci. 316, 713-745, https://doi.org/10.2475/08.2016.01, 2016.

Harland, R. and Nordberg, K.: The identification, occurrence and importance of microreticulate dinoflagellate cysts in the latest Holocene sediments of the Skagerrak and Kattegat, west coast of Sweden. Rev. Palaeobot. Palyno., 164, 84-92, https://doi.org/10.1016/j.revpalbo.2010.11.009, 2011.

965   HELCOM.: Water balance of the Baltic Sea, in: Baltic Sea Environment Proceedings, 16, The Baltic Marine Environment Protection Commission (eds.), Helsinki, Finland, 1986.

Henkes, G.A., Passey, B.H., Hopmans, E.C., Schouten, S., Pancost, R.D., van der Meer, M.T., Wanamaker, A.D., Grossman, E.L., Ambrose, W.G., and Carroll, M.L.: Carbonate clumped isotope compositions of modern marine mollusk and brachiopod shells. Geochim. Cosmochim. Ac., 106, 307-325, https://doi.org/10.1016/j.gca.2012.12.020, 2013.

970 Hopmans, E.C., Schouten, S., Pancost, R.D., van der Meer, M.T.J., and Sinninghe Damsté, J.S.: Analysis of intact tetraether lipids in archaeal cell material and sediments by high performance liquid chromatography/atmospheric pressure chemical ionization mass spectrometry. Rapid Commun. Mass Sp., 14, 585-589, https://doi.org/10.1002/(SICI)1097-0231(20000415)14:7<585::AID-RCM913>3.0.CO;2-N, 2000.

Hopmans, E.C., Weijers, J.W.H., Schefuß, E., Herfort, L., Sinninghe Damsté, J.S., and Schouten, S.: A novel proxy for
975 terrestrial organic matter in sediments based on branched and isoprenoid tetraether lipids. Earth Planet. Sc. Lett., 224, 107-116, https://doi.org/10.1016/j.epsl.2004.05.012, 2004.

Huckriede, H. and Meischner, D.: Origin and environment of manganese-rich sediments within black-shale basins. Geochim. Cosmochim. Ac., 60, 1399-1413, https://doi.org/10.1016/0016-7037(96)00008-7, 1996.

Hurrell, J.W.: Decadal trends in the North Atlantic Oscillation: Region Temperatures and Precipitation. Science, 269, 676-679
980 https://doi.org/10.1126/science.2695224.676, 1995.

ICES Hydrochemistry, CTD and Bottle data portal. ICES, Copenhagen, 2017.

Jakobsen, F. and Ottavi, J.: Transport through the contraction area in the Little Belt. Est., Coast., Shelf Sci. 45. 759-767, 1997.

IPCC, 2014: Climate Change 2014: Synthesis Report. Contribution of Working Groups I, II and III to the Fifth Assessment Report of the Intergovernmental Panel on Climate Change [Core Writing Team, R.K. Pachauri and L.A. Meyer (eds.)]. IPCC,
985 Geneva, Switzerland, 151 pp.

Iversen, J.: Viscum, Hedera and Ilex as Climate Indicators. Geol. Foren. Stock. For., 66, 463-483, https://doi.org/10.1080/11035894409445689, 1944.

Jonas, A.S., Schwark, L. Bauersachs, T.: Late Quaternary water temperature variations of the Northwest Pacific based on the lipid paleothermometers TEX$^H_{86}$, U$^{K'}_{37}$ and LDI. Deep Sea Research II 125, 81-93, 2017.

990 Kabel, K., Moros, M., Porsche, C., Neumann, T., Adolphi, F., Andersen, T.J., Siegel, H., Gerth, M., Leipe, T., Jansen, E.., and Sinninghe Damsté, J.S.: Impact of climate change on the Baltic Sea ecosystem over the past 1,000 years. Nat. Clim. Change, 2, 871-874, https://doi.org/10.1038/nclimate1595, 2012.

Keeling, R. F. and Garcia, H. E.: The change in oceanic O_2 inventory associated with recent global Warming. P. Natl. Acad. Sci., 99, 7848-7853, https://doi.org/10.1073/pnas.122154899, 2002.

995 Knudsen, K.L., Jiang, H., Gibbard, P.L., Kristensen, P., Seidenkrantz, M.-S., Janczyk-Kopikowa, Z., and Marks, L.: Environmental reconstructions of Eemian Stage interglacial marine records in the Lower Vistula area, southern Baltic Sea. Boreas, 41, 209-234, https://doi.org/10.1111/j.1502-3885.2011, 2011.

Kim, J.H., van der Meer, J., Schouten, S., Helmke, P., Willmott, V., Sangiorgi, F., Koc, N., Hopmans, E.C., and Sinninghe Damsté, J.S.: New indices and calibrations derived from the distribution of crenarchaeal isoprenoid tetraether lipids:

1000 Implications for past sea surface temperature reconstructions. Geochim. Cosmochim. Ac., 74, 4639-4654, https://doi.org/10.1016/j.gca.2010.05.027, 2010.

Kim, J.H., Romero, O.E., Lohmann, G., Donner, B., Laepple, T., Haam, E. and Sinninghe Damsté, J.S.: Pronounced subsurface cooling of North Atlantic waters off Northwest Africa during DAnsgaard-Oeschger interstadials. Earth Plan. Sc. Lett., 339-340, 95-102, 2012.

1005 Kotilainen, A.T., Arppe, L., Dobosz, S., Jansen, E., Kabel, K., Karhu, J., Kotilainen, M.M., Kuijpers, A., Lougheed, B.C., Meier, H.E.M., Moros, M., Neumann, T., Porsche, C., Poulsen, N., Rasmussen, P., Ribeiro, S., Risebrobakken, B., Ryabchuk, D., Schimanke, S., Snowball, I., Spiridonov, M., Virtasalo, J.J., Weckström, K., Witkowski, A., and Zhamoida, V.: Echoes from the Past: A Healthy Baltic Sea Requires More Effort. Ambio, 43, 60-68, https://doi.org/10.1007/s13280-013-0477-4, 2014.

1010 Kotthoff, U., Pross J., Müller U.C., Peyron O., Schmiedl G., Schulz H., and Bordon A.: Climate dynamics in the borderlands of the Aegean Sea during formation of sapropel S1 deduced from a marine pollen record. Quaternary Sci. Rev., 27, 832-845, https://doi.org/10.1016/j.quascirev.2007.12.001, 2008.

Kotthoff, U., Koutsodendris, A., Pross, J., Schmiedl, G., Bornemann, A., Kaul, C., Marino, G., Peyron, O., and Schiebel, R.: Impact of late glacial cold events in the Northern Aegean region reconstructed from integrated marine and terrestrial proxy

1015 data. J. Quaternary Sci., 26, 86-96, https://doi.org/10.1002/jqs.1430, 2011.

Krammer, K., & Lange-Bertalot, H.: Bacillariophyceae, Part 1. Naviculaceae. Süßwasserflora von Mitteleuropa (Vol. 2/1), Ettl, H., Gerloff, J., Heynig, H., and Mollenhauer, D. (Eds.), Gustav Fischer Verlag, Stuttgart, Germany, 876 pp. 1986.

Krammer, K., & Lange-Bertalot, H.: Bacillariophyceae, Part 2. Bacillariaceae, Epithemiaceae, Surirellaceae. Süßwasserflora von Mitteleuropa (Vol. 2/2), Ettl, H., Gerloff, J., Heynig, H., & Mollenhauer, D. (Eds.), Gustav Fischer Verlag, Stuttgart,

1020 Germany, 611 pp., 1988.

Krammer, K., & Lange-Bertalot, H.: Bacillariophyceae, Part 3. Centrales, Fragilariaceae, Eunotiaceae. Süßwasserflora von Mitteleuropa (Vol. 2/3), Ettl, H., Gerloff, J., Heynig, H., & Mollenhauer, D. (Eds.), Gustav Fischer Verlag, Stuttgart, 598 pp., 1991a.

Krammer, K., & Lange-Bertalot, H.: Bacillariophyceae, Part 4. Achnantaceae. Süßwasserflora von Mitteleuropa (Vol. 2/4),

1025 Ettl, H., Gerloff, J., Heynig, H., & Mollenhauer, D. (Eds.), Gustav Fischer Verlag, Stuttgart, 468 pp., 199b.

Kristensen, P.H. and Knudsen, K.L.: Palaeoenvironments of a complete Eemian sequences at Mommark, South Denmark: foraminifera, ostracods and stable isotopes. Boreas, 35. 349-366, https://doi.org/10.1111/j.1502-3885.2006.tb01163.x, 2006.

Kristjánsdóttir, G.B., Lea, D.W., Jennings, A.E., Pak, D.K., Belanger, C.: New spatial Mg/Ca-temperature calibrations for three Arctic, benthic foraminifera and reconstruction of north Iceland shelf temperature for the past 4000 years. Geochem.,

1030 Geophys., Geosys., 8, Q03P21, https://doi.org/10.1029/2006GC001425, 2007.

Krossa, V.R., Moros, M., Leduc, G., Hinz, M., Blanz, T., and Schneider, R.: Regional climate change and the onset of farming in northern Germany and southern Scandinavia. The Holocene, https://doi.org/10.1177/0959683617702223, 2017.

Kühl, N., Moschen, R.: A combined pollen and $\delta^{18}O_{Sphagnum}$ record of mid-Holocene climate variability from Dürres Maar (Eifel, Germany). The Holocene, 22, 1075-1085, https://doi.org/10.1177/0959683612441838, 2012.

1035 Leppäranta, M. and Myrberg, K.: Physical oceanography of the Baltic Sea. Springer-Verlag Berlin Heidelberg, 378 pp., 2009.

Liu, X.L., Summons, R.E., and Hinrichs, K.U.: Extending the known range of glycerol ether lipids in the environment: structural assignments based on tandem mass spectral fragmentation patterns. Rapid Commun. Mass Sp., 26, 2295-2302, https://doi.org/10.1002/rcm.6355, 2012.

Lopes dos Santos, R.A., Spooner, M.I., Barrows, T.T., De Deckker, P., Sinninghe Damsté, J.S., and Schouten, S.: Comparison

1040 of organic ($U^{K'}_{37}$, TEX^{H}_{86}, LDI) and faunal proxies (foraminiferal assemblages) for reconstruction of late Quaternary sea surface temperature variability from offshore southeastern Australia. Paleoceanography, 28, 377-387, https://doi.org/10.1002/palo.20035, 2013.

Lutze, G.: Zur Foraminiferen-Fauna der Ostsee. Meyniana, 15, 75–142, https://doi.org/10.2312/meyniana.1965.15.75, 1965.

Lutze, G.: Foraminiferen der Kieler Bucht (Westliche Ostsee): 1 'Hausgartengebiet' des Sonderforschungsbereiches 95 der

1045 Universität Kiel. Meyniana, 26, 9-22, https://doi.org/10.2312/meyniana.1974.26.9, 1974.

Martin, P.A. and Lea, D.W.: simple evaluation of cleaning procedures on fossil benthic foraminiferal Mg/Ca. Geochem., Geophys., Geosys., 3. 1-8, https://doi.org/10.1029/2001GC000280, 2002.

Matthäus, W. and Schinke, H.: The influence of river runoff on deep water conditions of the Baltic Sea. Hydrobiologia, 393, 1-10, https://doi.org/10.1023/A:1003573328473, 1999.

1050 Mauri, A., Davis, B.A.S., Collins, P.M., and Kaplan, J.O.: The Climate of Europe during the Holocene: a gridded pollen-based reconstruction and its multi-proxy evaluation. Quaternary Sci. Rev., 112, 109-127, https://doi.org/10.1016/j.quascirev.2015.01.013, 2015.

Meier, H.E.M., Feistel, R., Piechura, J., Arneborg, L., Burchard, H., Fiekas, V., Golenko N., Kuzmina, N., Mohrholz, V., Nohr, C., Paka; V.T., Sellschopp, J., Stips, A., Zhurbas, V.: Ventilation of the Baltic Sea deep water: A brief review of present

1055 knowledge from observations and models. Oceanologia, 48(S): 133-164, 2006.

Meier, H.E.M., Müller-Karulis, B., Andersson, H.C., Dieterich, C., Eilola, K., Gustafsson, B.G., Höglund, A., Hordoir, R., Kuznetsov, I., Neumann, T., Ranjbar, Z., Savchuk, O.P., and Schimanke, S.: Impact of Climate Change on Ecological Quality Indicators and Biogeochemical Fluxes in the Baltic Sea: A Multi-Model Ensemble Study. Ambio, 41:558–573, https://doi.org/10.1007/s13280-012-0320-3, 2012.

1060 Meier, H.E.M.: Projected Change – Marine Physics, In: Second Assessment of Climate Change for the Baltic Sea Basin, Bolle, H.-J., Massimo Menenti, S., al Vesuvio, S./The BACC Author Team (eds.), Springer, 243-252, https://doi.org/10.1007/978-3-319-16006-1, 2015.

Michalak, A.M., Anderson, E.J., Beletsky, D., Boland, S., Bosch, N.S., Bridgeman, T.B., Chaffin, J.D., Cho, K., Confesor, R., Daloğlu, I., DePinto, J.V., Evans, M.A., Fahnenstiel, G.L., He, L., Ho, J.C., Jenkins, L., Johengen, T.H., Kuo, K.C., LaPorte,

1065 E., Liu, X., McWilliams, M.R., Moore, M.R., Posselt, D.J., Richards, R.P., Scavia, D., Steiner, A.L., Verhamme, E., Wright, D.M., and Zagorski, M.A.: Record-setting algal bloom in Lake Erie caused by agricultural and meteorological trends consistent

with expected future conditions. P. Natl. Acad. Sci. USA., 110 (16), 6448-6452, https://doi.org/10.1073/pnas.1216006110, 2013.

Mohrholz, V., Naumann, M., Nausch, G., Krüger, S., and Gräwe, U.: Fresh oxygen for the Baltic Sea - An exceptional saline inflow after a decade of stagnation. J. Mar. Sys., 148, 152-166, https://doi.org/10.1016/j.jmarsys.2015.03.005, 2015.

Mudie, P.J., Rochon, A., Aksu, A.E., and Gillespie, H.: Dinoflagellate cysts, freshwater algae and fungal spores as salinity indicators in Late Quaternary cores from Marmara and Black seas. Mar. Geol., 190, 203-231, https://doi.org/10.1016/S0025-3227(02)00348-1, 2002

Murray, J.W.: Ecology and Applications of Benthic Foraminifera. Cambridge University Press, 440 pp., 2006.

Ning, W., Anderson, P.S., Ghosh, A., Khan, M., and Filipsson, H.L.: Quantitative salinity reconstructions of the Baltic Sea during the mid-Holocene. Boreas, https://doi.org/10.11111/bor.12156. ISSN 0300-9483, 2015.

Ning, W., Ghosh, A., Jilbert, T., Slomp, J.P., Khan, M., Nyberg, J., Conley, D.J., and Filipsson, H.L.: Evolving coastal character of a Baltic Sea inlet during the Holocene shoreline regression: impact on coastal zone hypoxia. J. Paleolimnol., 55, 319-338, https://doi.org/10.1007/s10933-016-9882-6, 2016.

Ning, W., Andersson, P.S., Ghosh, A., Khan, M., Filipsson, H.L.: Quantitative salinity reconstructions of the Baltic Sea during the mid-Holocene. Boreas 46, 100-110, https://doi.org/10.1111/bor.12156, 2017.

O'Neil, J.M., Davis, T.W., Burford, M.A., and Gobler, C.J.: The rise of harmful cyanobacteria blooms: The potential roles of eutrophication and climate change. Harmful Algae, 14, 313-334, https://doi.org/10.1016/j.hal.2011.10.027, 2012.

Omstedt, A., Meuller, L., and Nyberg, L.: Interannual, seasonal, and regional variations of precipitation and evaporation over the Baltic Sea. Ambio, 26, 484-492, 1997.

Osterman, L. E., Poore, R. Z., Swarzenski, P. W., and Turner, R. E.: Reconstructing a 180 yr record of   natural   and anthropogenic induced low-oxygen conditions from Louisiana continental shelf sediments. Geology, 33, 329-332, https://doi.org/10.1130/G21341.1, 2005.

Passey, B. H., Levin, N.E., Cerling, T.E., Brown, F.H., Eiler, J.M.., and Rendle-Bürhing, R., 2010. High-temperature environments of human evolution in East Africa based on bond ordering in paleosol carbonates. P. Natl. Acad. Sci. USA, 107, 11245-11249, https://doi.org/10.1073/pnas.1001824107, 2010.

Patrick, R., and Reimer, C.W.: The Diatoms of the United States. Monographs of the Natural Academy of Sciences of Philadelphia, Number 13, 688 pp, https://doi.org/10.1002/iroh.19680530120, 1966.

Platon, E., Sen Gupta, B.K., Rabalais, N.N., and Turner, R.E.: Effect of seasonal hypoxia on the benthic foraminiferal community of the Louisiana inner continental shelf: The 20th century record. Mar. Micropaleontol., 54, 263-283, https://doi.org/10.1016/j.marmicro.2004.12.004, 2005.

Powers, L., Werne, J. P., Vanderwoude, A. J., Sinninghe Damsté, J.S., Hopmans, E. C., and Schouten, S.: Applicability and calibration of the TEX86 paleothermometer in lakes. Org. Geochem., 41, 404–413, doi:10.1016/j.orggeochem.2009.11.009, 2010.

Raiswell, R., Canfield, D.E.: Sources of iron for pyrite formation in marine sediments. Am. J. Sci. 298, 219-245, 1998.

Raitzsch, M., Kuhnert, H., Groeneveld, J., and Bickert, T.: Benthic foraminifer Mg/Ca anomalies in South Atlantic core top sediments and their implications for paleothermometry. Geochem., Geophys., Geosys., 9, Q05010, https://doi.org/10.1029/2007GC001788, 2008.

Rampen, S.W., Willmott, V., Kim, J.-H., Uliana E., Mollenhauer, G., Schefuß E., Sinninghe Damsté, J.S., and Schouten, S.:

1105 Long chain 1,13- and 1,15-diols as a potential proxy for palaeotemperature reconstruction. Geochim. Cosmochim. Ac., 84, 204-216, https://doi.org/10.1016/j.gca.2012.01.024, 2012.

Rampen, S.W., Datema, M., Rodrigo-Gámiz, M., Schouten, S., Reichart, G.J., and Sinninghe Damsté, J.S.: Sources and proxy potential of long chain alkyl diols in lacustrine environments. Geochim. Cosmochim. Ac., 144, 59-71, https://doi.org/10.1016/j.gca.2014.08.033, 2014.

1110 Reimer, P.J., Bard, E., Bayliss, A., Beck, J.W., Blackwell, P.G., Bronk Ramsey, C., Buck, C.E., Cheng, H., Edwards, R.L., Friedrich, M., Grootes, P.M., Guilderson, T.P., Haflidason, H., Hajdas, I., Hatté, C., Heaton, T.J., Hoffmann, D.L., Hogg, A.G., Hughen, K.A., Kaiser, K.F., Kromer, B., Manning, S.W., Niu, M., Reimer, R.W., Richards, D.A., Scott, E.M., Southon, J.R., Staff, R.A., Turney, C.S.M., and van der Plicht, J.: IntCal13 and Marine13 radiocarbon age calibration curves 0-50,000 years cal BP. Radiocarbon, 55, 1869-1887, https://doi.org/10.2458/azu_js_rc.55.16947, 2013.

1115 Rodrigo-Gámiz, M., Rampen, S.W., de Haas, H., Baas, M., Schouten, S., and Sinninghe Damsté, J.S. Constraints on the applicability of the organic temperature proxies $U^{K'}_{37}$, TEX_{86} and LDI in the subpolar region around Iceland. Biogeosciences, 12, 6573-6590, https://doi.org/10.5194/bg-12-6573-2015, 2015.

Rütters, H., Sass, H., Cypionka, H., and Rullkötter, J.: Phospholipid analysis as a tool to study complex microbial communities in marine sediments. J. Microbiol. Meth., 48, 149-160, https://doi.org/10.1016/S0167-7012(01)00319-0, 2002.

1120 Schöne, B.R.: The curse of physiology–challenges and opportunities in the interpretation of geochemical data from mollusk shells. Geo.-Mar. Lett., 28, 269-285, https://doi.org/10.1007/s00367-008-0114-6, 2008.

Schouten, S., Hopmans, E.C., Schefuß, E., and Sinninghe Damsté, J.S.: Distributional variations in marine crenarchaeotal membrane lipids: a new tool for reconstructing ancient sea water temperatures?. Earth Planet. Sc. Lett., 204, 265-274, https://doi.org/10.1016/S0012-821X(02)00979-2, 2002.

1125 Schouten, S., Hopmans, E.C., Rosell-Melé, A., Pearson, A., Adam, P. et. al. An interlaboratory study of TEX_{86} and BIT analysis of sediments, extracts, and standard mixtures. Geochem., Geophys., Geosys., 14, 1-23, https://doi.org/10.1002/2013GC004904, 2013a.

Schouten, S., Hopmans, E.C., and Sinninghe Damsté, J.S.: The organic geochemistry of glycerol dialkyl glycerol tetraether lipids: a review. Org. Geochem.. 54, 19-61, https://doi.org/10.1016/j.orggeochem.2012.09.006, 2013b.

1130 Seidenkrantz, M.-S.: Subrecent changes in the foraminiferal distribution in the Kattegat and the Skagerrak, Scandinavia: anthropogenic influence and natural causes. Boreas. 22 (4), 383-395, https://doi.org/10.1111/j.1502-3885.1993.tb00201.x, 1993.

Seppä, H., Hammarlund, D., and Antonsson, K.: Low-frequency and high-frequency changes in temperature and effective humidity during the Holocene in south-central Sweden: implications for atmospheric and oceanic forcings of climate. Clim. Dynam., 25, 285-297, https://doi.org/10.1007/s00382-005-0024-5, 2005.

Shen, C.-C., Hastings, D.W., Lee, T., Chiu, C.-H., Lee, M.-Y., Wei, K.-Y., and Edwards, R.L.: High precision glacial-interglacial benthic foraminiferal Sr/Ca records from the eastern Atlantic Ocean and Caribbean Sea. Earth Plan. Sci. Lett., 190. 197-209, https://doi.org/10.1016/S0012-821X(01)00391-0, 2001.

Skirbekk, K., Hald, M., Marchitto, T.M., Junttila, J., Kristensen, D.K., and Sörensen, S.A.: Benthic foraminiferal growth seasons implied from Mg/Ca-temperature correlations for three Arctic species. Geochem., Geophys., Geosys., 17, 4684-4704, https://doi.org/10.1002/2016GC006505, 2016.

Snoeijs, P.: Intercalibration and distribution of diatom species in the Baltic Sea. Volume 1. OPULUS Press, Uppsala, 130 pp., 1993.

Snoeijs, P. & Vilbaste, S.: Intercalibration and distribution of diatom species in the Baltic Sea. Voulme 2. OPULUS Press, Uppsala. 125 pp., 1994.

Snoeijs, P. & Potapova, M.: Intercalibration and distribution of diatom species in the Baltic Sea. Volume 3. OPULUS Press, Uppsala. 125 pp., 1995.

Snoeijs, P. & Kasperoviciene, J.: Intercalibration and distribution of diatom species in the Baltic Sea. Volume 4. OPULUS Press, Uppsala. 125 pp., 1996.

Snoeijs, P., & Balashova, N.: Intercalibration and distribution of diatom species in the Baltic Sea. Volume 5. OPULUS Press, Uppsala. 144 pp., 1998.

Snoeijs, P. and Weckström, K.: Diatoms and environmental change in large brackish-water ecosystems. In: The Diatoms: Applications for the Environmental and Earth Sciences, 2, Smol, J.P. and Stoermer, E.F. (eds), Cambridge University Press, 287-308, https://doi.org/10.1017/CBO9780511763175.016, 2010.

Sohlenius, G., Sternbeck, J., Andrén, E., and Westman, P.: Holocene history of the Baltic Sea as recorded in a sediment core from the Gotland Deep. Mar. Geol., 134, 183-201, https://doi.org/10.1016/0025-3227(96)00047-3, 1996.

Steinke, S., Groeneveld, J., Johnstone, H., and Rendle-Bürhing, R.: East Asian summer monsoon weakening after 7.5 Ma: Evidence from combined planktonic foraminifera Mg/Ca and δ^{18}O (ODP Site 1146; northern South China Sea). Palaeogeogr. Palaeocl., 289. 33-43, https://doi.org/10.1016/j.palaeo.2010.02.007, 2010.

Stepanova, A., Taldenkova, E., Simstich, J., and Bauch, H.A.: Comparison study of the modern ostracod associations in the Kara and Laptev seas: Ecological aspects. Mar. Micropaleontol., 63, 111-142, https://doi.org/10.1016/j.marmicro.2006.10.003, 2007.

Stockmarr, J.: Tablets with spores used in absolute pollen analysis. Pollen et Spores, 13, 615–21, 1971.

Thorsen, T.A., Dale, B., and Nordberg, K.: 'Blooms' of the toxic dinoflagellate *Gymnodinium catenatum* as evidence of climatic fluctuations in the late Holocene of southwestern Scandinavia. The Holocene, 5, 435-446, https://doi.org/10.1177/095968369500500406, 1995.

Thorsen, T.A., and Dale, B.: Dinoflagellate cysts as indicators of pollution and past climate in a Norwegian fjord. The Holocene, 7, 433-446, https://doi.org/10.1177/095968369700700406, 1997.

Van Helmond, N.A.G.M., Krupinski, N.Q., Lougheed, B.C., Obrochta, S.P., Andrén, T., and Slomp, C.P.: Seasonal hypoxia was a natural feature of the coastal zone in the Little Belt, Denmark, during the past 8 ka. Marine Geology, 387, 45-57, https://doi.org/10.1016/j.margeo.2017.03.008, 2017.

Van Santvoort, P.J.M., De Lange, G.J., Thomson, J., Colley, S., Meysman, F.J.R., and Slomp, C.P.: Oxidation and origin of organic matter in surficial eastern Mediterranean hemipelagic sediments. Aquatic Geochemistry, 8, 153-175. https://doi.org/10.1023/A:1024271706896. 2002.

de Vernal, A. and Marret, F.: Organic-walled dinoflagellate cysts: tracers of sea-surface conditions, In: Proxies in Late Cenozoic Paleoceanography, Hillaire-Marcel, C. and de Vernal, A. (eds.), Elsevier, 371-408, https://doi.org/10.1016/S1572-5480(07)01014-7, 2007.

Versteegh, G.J.M., Bosch, H.J., and de Leeuw, J.W.: Potential palaeoenvironmental information of C_{24} to C_{36} mid-chain diols, keto-ols and mid-chain hydroxy fatty acids; a critical review. Org. Geochem., 27, 1-13, https://doi.org/10.1016/S0146-6380(97)00063-6, 1997.

Viehberg, F.A., Frenzel, P., and Hoffmann, G.: Succession of late Pleistocene and Holocene ostracode assemblages in a transgressive environment: A study at a coastal locality of the southern Baltic Sea (Germany). Palaeogeogr. Palaeoclim., 264, 318-329, https://doi.org/10.1016/j.palaeo.2007.05.026, 2008.

Visbeck, M.H., Hurrel, J.W., Polvani, L., and Cullen, H.M.: The North Atlantic Oscillation: Past, present, and future. P. Natl. Acad. Sci. USA, 98, 12876-12877, https://doi.org/10.1073/pnas.231391598, 2001.

Volkman, J.K., Barrett, S.M., Dunstan, G.A., and Jeffrey, S.W.: C_{30}-C_{32} alkyl diols and unsaturated alcohols in microalgae of the class Eustigmatophyceae. Org. Geochem., 18, 131-138, https://doi.org/10.1016/S0146-6380(99)00009-1, 1992.

Volkman, J.K., Barrett, S.M., and Blackburn, S.I.: Eustigmatophyte microalgae are potential sources of C_{29} sterols, C_{22}-C_{28} *n*-alcohols and C_{28}-C_{32} *n*-alkyl diols in freshwater environments. Org. Geochem., 30, 307-318, https://doi.org/10.1016/S0146-6380(99)00009-1, 1999.

Wacker, U., Fiebig, J., Tödter, J., Schöne, B.R., Bahr, A., Friedrich, O., Tütken, T., Gischler, E., and Joachimski, M.M,: Empirical calibration of the clumped isotope paleothermometer using calcites of various origins. Geochim. Cosmochim. Ac., 141, 127-144, https://doi.org/10.1016/j.gca.2014.06.004, 2014.

Warnock, J.P., and Scherer, R.P.: A revised method for determining the absolute abundance of diatoms. J. Paleolimnol., 53, 157-163, https://doi.org/10.1007/s10933-014-9808-0, 2015.

Warnock, J., Andrén, E., Bauersachs, T., Brandt, H.-T., Kotthoff, U.: Holocene environmental history of the Ångermanälven Estuary, northern Baltic Sea. Boreas, DOI: 10.1111/bor.12281, 2017.

Wasmund, N., and Uhlig, S.: Phytoplankton trends in the Baltic Sea. ICES J. Mar. Sci., 60, 177-186, https://doi.org/10.1016/S1054-3139(02)00280-1, 2003.

1200 Weijers, J.W.H., Schouten, S., Spaargaren, O.C., and Sinninghe Damsté, J.S.: Occurrence and distribution of tetraether membrane lipids in soils: implications for the use of the TEX$_{86}$ proxy and BIT index. Org. Geochem., 37, 1680-1693, https://doi.org/10.1016/j.orggeochem.2006.07.018, -2006.

Weijers, J.W.H., Lim, K.L.H., Aquilina, A., Sinninghe Damsté, J.S., and Pancost, R.D.: Biogeochemical controls on glycerol dialkyl glycerol tetraether lipid distributions in sediments characterized by diffusive methane flux. Geochem., Geophys.,
1205 Geosys., 12, https://doi:10.1029/2011GC003724, 2011.

Willumsen, P.S., Filipsson, H.L., Reinholdsson, M., and Lenz, C.; Surface salinity and nutrient variations during the Littorina Stage in the Fårö Deep, Baltic Sea. Boreas, 42, 210-223, https://doi.org/10.1111/j.1502-3885.2012.00286x, 2013.

Yu, S.-Y., Berglund, B.-E.: A dinoflagellate cyst record of Holocene climate and hydrological changes along the southeastern Swedish Baltic coast. Quaternary Res., 67, 215–224, https://doi.org/10.1016/j.yqres.2006.12.004, 2007.

1210 Zhang, Y.G., Zhang, C.L., Liu, X.L., Li, L., Hinrichs, K.U., Noakes, J.E.: Methane Index: A tetraether archaeal lipid biomarker indicator for detecting the instability of marine gas hydrates. Earth Plan. Sc. Lett., 307, 525-534, 2011.

Zhu, C., Weijers, J.W.H., Wagner, T., Pan, J.M., Chen, J.F., and Pancost, R.D.: Sources and distributions of tetraether lipids in surface sediments across a large river-dominated continental margin. Org. Geochem., 42, 376-386, https://doi.org/10.1016/j.orggeochem.2011.02.002, 2011.

1215 Zillén, L., Conley, D.J., Andrén, T., Andrén, E., and Björck, S.: Past occurrences of hypoxia in the Baltic Sea and the role of climate variability, environmental change and human impact. Earth-Sci. Rev., 91, 77-92, https://doi.org/10.1016/j.earscirev.2008.10.001, 2008.

Zink, K.G, Vandergoes, M.J., Bauersachs, T., Newnham, R.M., Rees, A.B.H., and Schwark, L.: A refined paleotemperature calibration for New Zealand limnic environments using differentiation of branched glycerol dialkyl glycerol tetraether
1220 (brGDGT) sources. J. Quat. Sci., 31, 823-835, https://doi.org/10.1002/jqs.2908, 2016.

Zonneveld, K.A.F. and Pospelova V.: A determination key for modern dinoflagellate cysts. Palynology, 39, 387- 409, https://doi.org/10.1080/01916122.2014.990115, 2015.
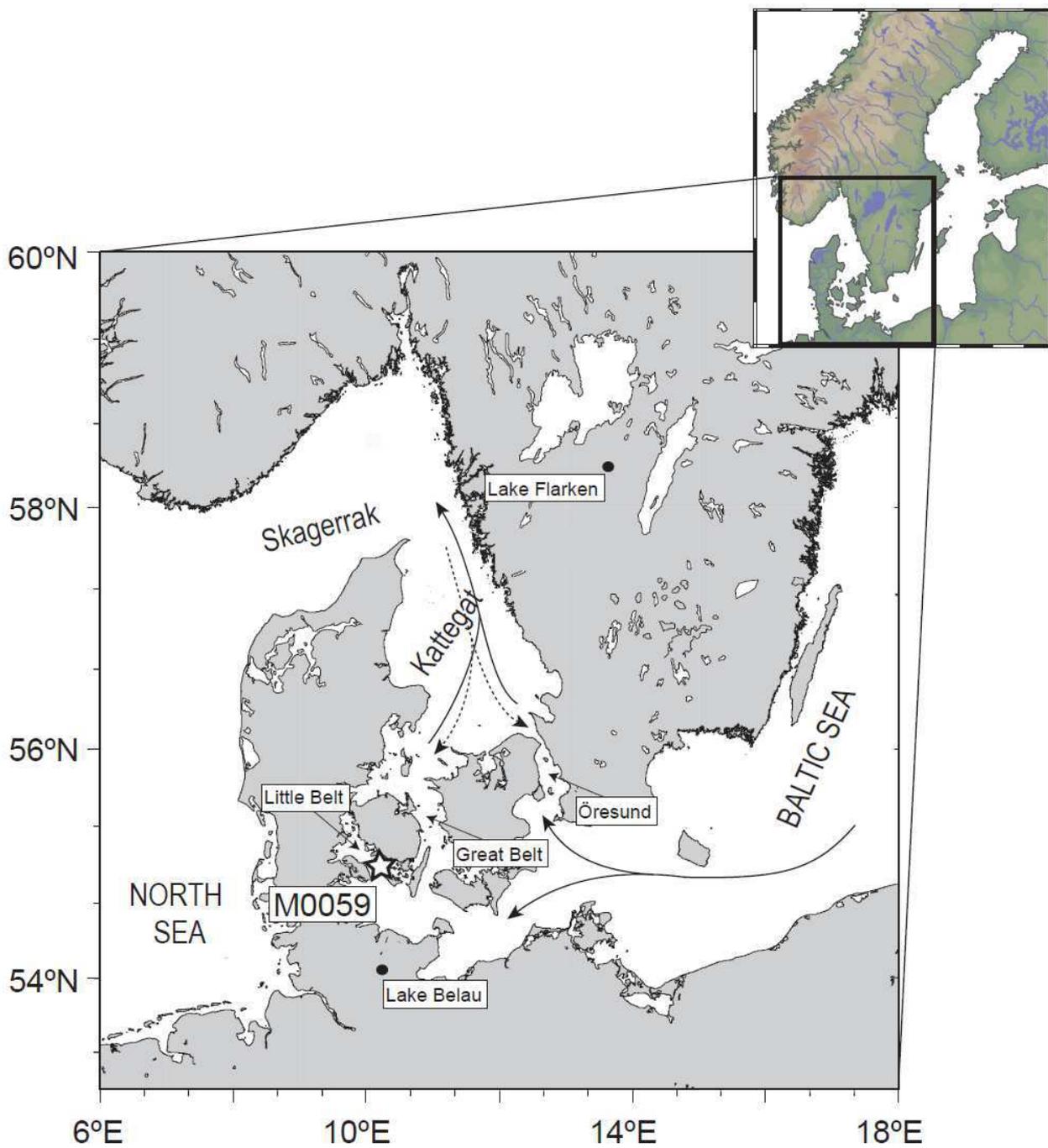
1225 **Figure 1: Map of the southern Baltic Sea (redrawn from Groeneveld and Filipsson, 2013). The positions of IODP Site M0059 (white star; 55°0.29′N29′N, 10°6.49′E49′E; Andrén et al., 2015a), Lake Belau (Dörfler et al., 2012), and Lake Flarken (Seppä et al., 2005) are indicated. Continuous (surface) and dashed (bottom) lines indicate dominant current directions.**

Fig. 2
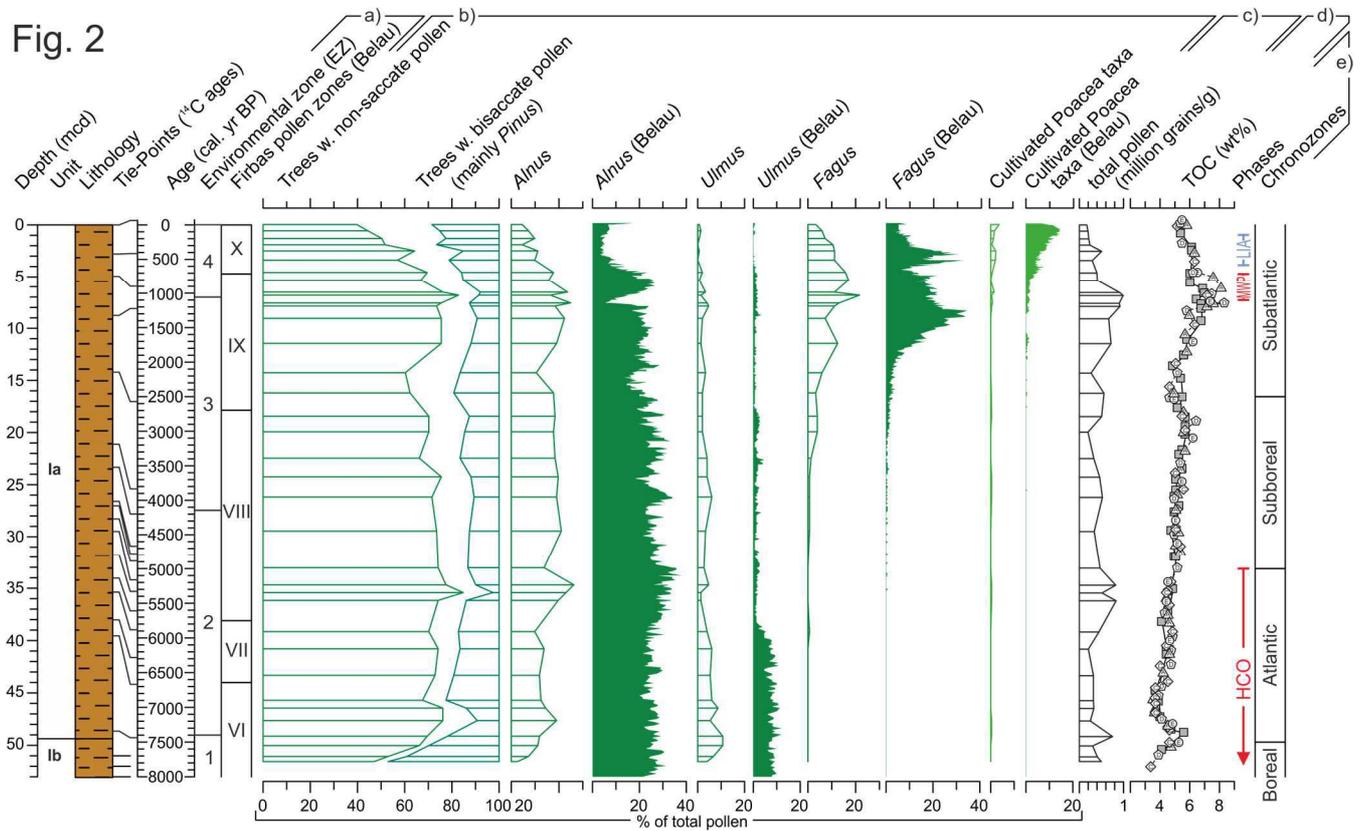
Figure 2: Comparison of the pollen record from IODP Site M0059 with the varved pollen record of Lake Belau (northern Germany, Dörfler et al., 2012). Sedimentological units, lithology (Andrén et al., 2015a), position of ¹⁴C ages (Van Helmond et al., 2017) plotted vs. depth; plotted vs. age (extrapolated below ~48.64 mcd): a) environmental zones (EZ; IODP Site M0059), Firbas pollen zones (Lake Belau), b) selected pollen taxa (w. horizontal bars: IODP Site M0059, filled: Lake Belau), c) total organic carbon (TOC; white: shipboard data – triangles: Hole A, rhombi: Hole C, pentagons: Hole D, circles: Hole E; grey squares: onshore data) for IODP Site M0059, d) climate phases and chronozones.

1230

1235   Fig. 3
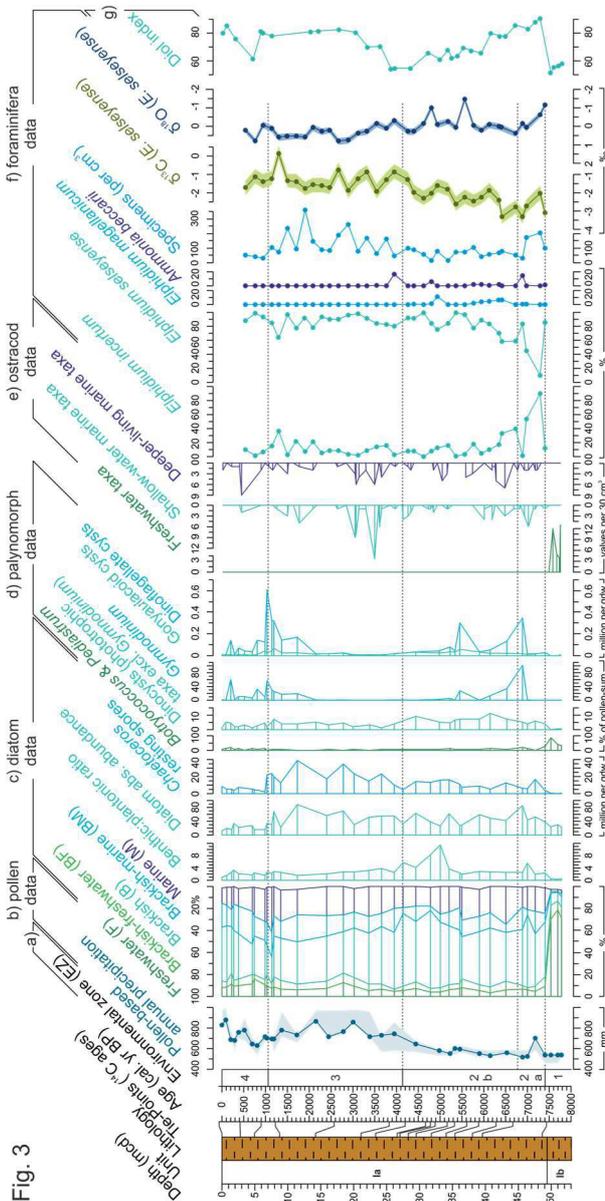
Figure 3: Sedimentological units, lithology (Andrén et al., 2015a), position of ^{14}C ages (Van Helmond et al., 2017) vs. depth; IODP Site M0059 precipitation and salinity proxies plotted vs. age (extrapolated below ~48.64 mcd): a) environmental zones (EZs) based on diatom data; b) pollen-based precipitation reconstructions based on the modern analogues technique; c) diatom salinity-based
1240   **affinities and life forms (benthic vs. pelagic) following Snoeijs et al. (1993-1998) with species assignments provided** ~~table S5~~ **Table S2 in the supplement; d) palynomorphs/pollen ratios based on total amount of terrestrial pollen, freshwater algae comprising *Botryococcus* and *Pediastrum* species, dinocysts predominately comprising cysts of *Protoceratium reticulatum* (*Operculodinium* cysts), *Lingulodinium*, and *Spiniferites* species (*Gymnodinium* excluded); e) Ostracod shallow water/deeper living marine taxa plotted from right to left; f) total abundance of benthic foraminifera per cm³ of dried sediment with the relative abundance of the most common species; benthic foraminiferal taxa (*Elphidium incertum*, *E. selseyense*, *E. magellanicum,* and *Ammonia beccarii*) shown as % of total**
1245   **benthic foraminiferal fauna; total abundance of benthic foraminifera shown as specimens per cm³ of dried sediment; stable carbon and oxygen isotope data analysed on *E. selseyense*; g) Diol Index indicating relative changes in surface water salinity.**

Fig. 4
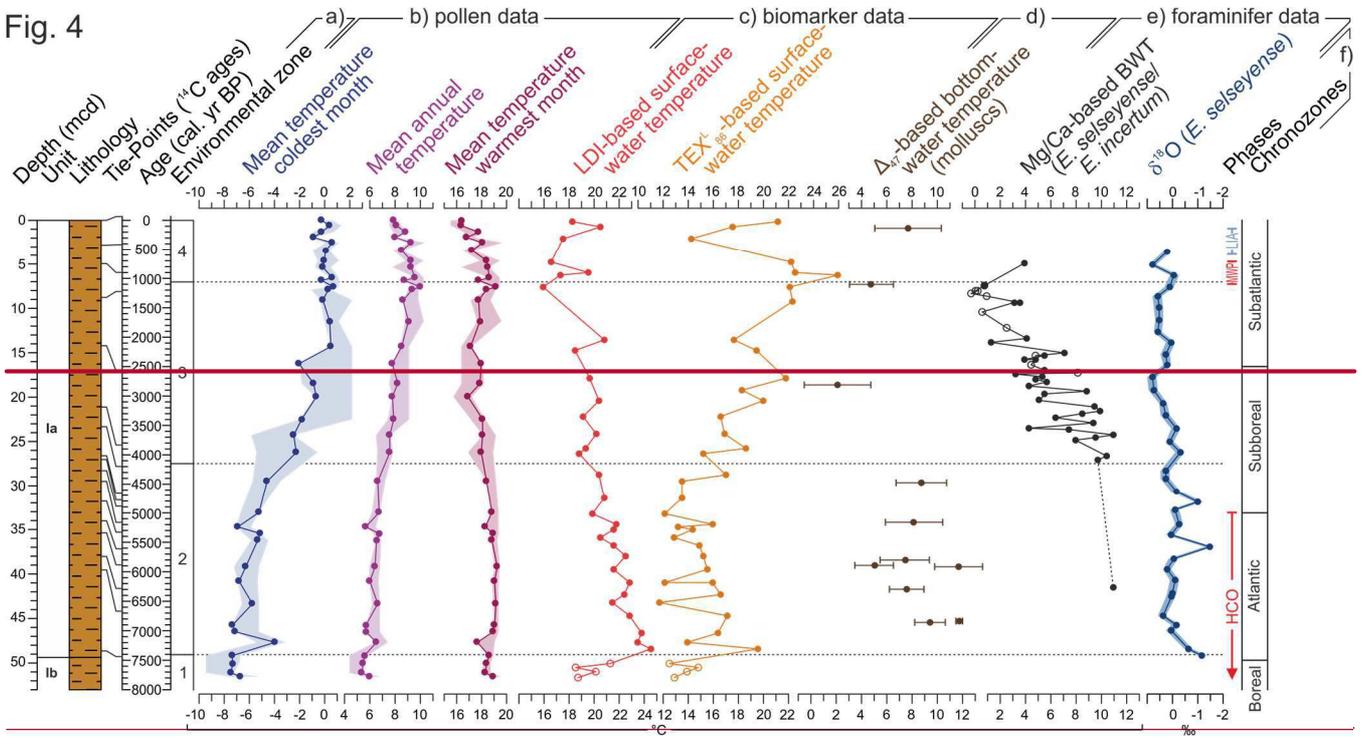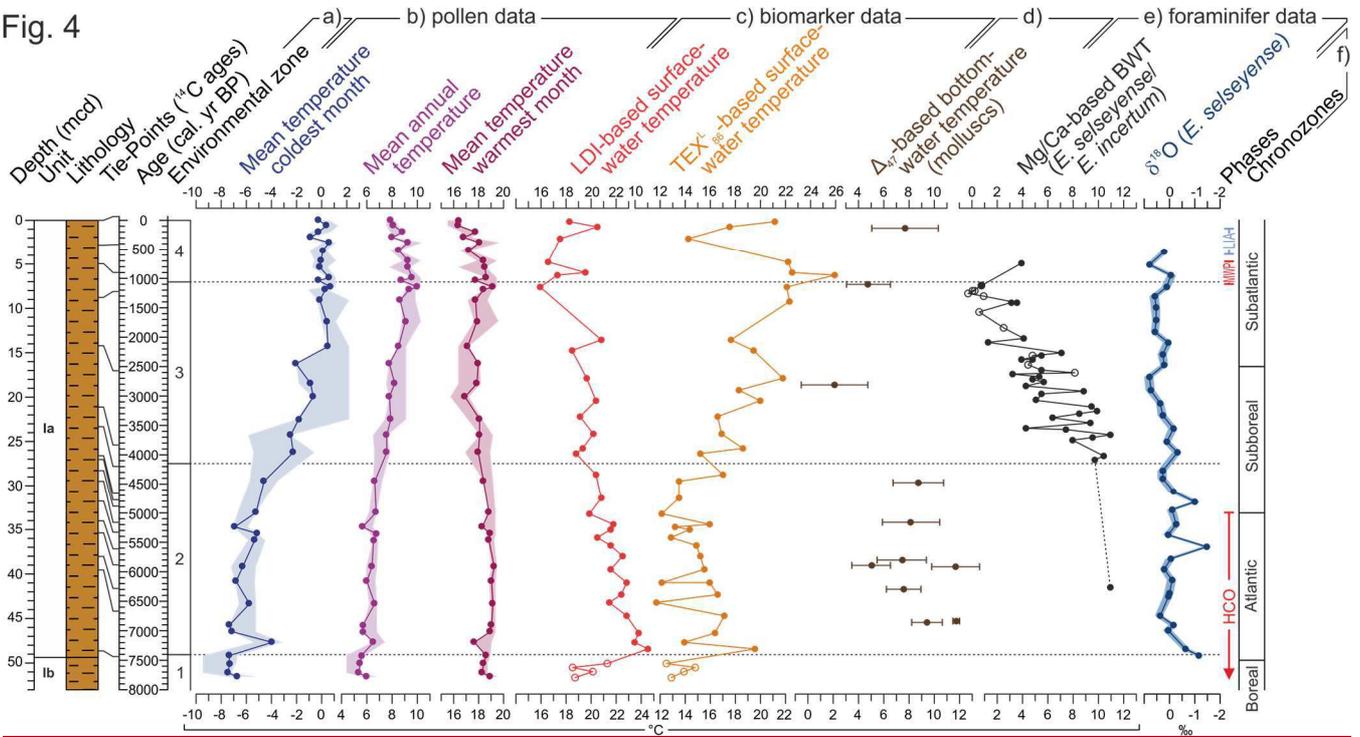
Figure 4: Sedimentological units, lithology (Andrén et al., 2015a), position of ^{14}C ages (Van Helmond et al., 2017) vs. depth; IODP Site M0059 temperature proxies plotted vs. age (extrapolated below ~48.64 mcd): a) environmental zones (EZs) based on diatom data; b) pollen-inferred climate reconstructions based on the modern analogues technique, shaded area reflects the range of the best 10 analogues; c) Long-chain-diol-index (LDI)- and TEX$^L_{86}$-reconstructed SSTs both reflecting a summer signal; d) Δ$_{47}$-inferred temperatures based on clumped isotope composition of mollusc shells; e) Mg/Ca-based bottom water temperature (BWT) reconstructed using the benthic foraminifera *E. selseyense* and *E. incertum*; stable oxygen isotopes based on the benthic foraminifer *E. selseyense*; f) climate phases and chronozones.

Fig. 5
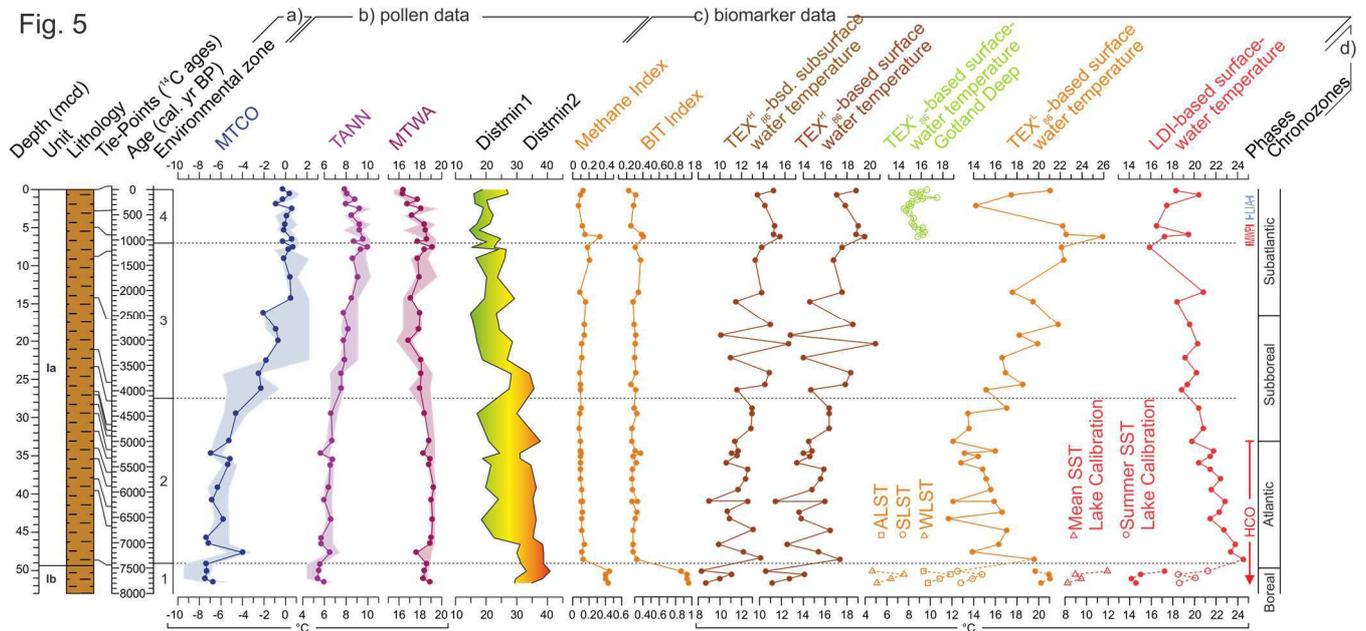
Fig. 5: Sedimentological units, lithology (Andrén et al., 2015a), position of ^{14}C ages (Van Helmond et al., 2017) vs. depth; IODP Site M0059 temperature proxies and related datasets plotted vs. age (extrapolated below ~48.64 mcd): a) environmental zones (EZs) based on diatom data; b) pollen-inferred climate reconstructions based on the modern analogues technique, shaded area reflects the range of the best eight analogues, Distmin1/Distmin2: squared chord distance between fossil sample and best/8th-best modern analogue, indicating similarity between fossil and modern samples; c) methane and branched isoprenoid tetraether (BIT) indices, TEX$^H_{86}$-based subsurface water temperature, TEX$^H_{86}$-based surface water temperature, TEX$^L_{86}$-based surface water temperature from the Gotland Deep (Kabel et al., 2012) for comparison, TEX$^L_{86}$-based surface water temperatures, shown with lake calibrations for EZ1 (ALST = annual, SLST = summer, WLST = winter lake surface temperatures (after Powers et al. 2010) and long-chain-diol-index-based (LDI-based) sea surface temperatures with lake callibrations for EZ; (after Rampen et al., 2014); d) climate phases and chronozones.